ROYAL SOCIETY OF CHEMISTRY

Chem Soc Rev

Construction of multiferrocenyl metallacycles and metallocages via coordination-driven self-assembly: from structure to functions

Journal:	*Chemical Society Reviews*
Manuscript ID:	CS-TRV-01-2015-000022.R1
Article Type:	Tutorial Review
Date Submitted by the Author:	16-Feb-2015
Complete List of Authors:	Xu, Lin; East China Normal University, Shanghai Key Labs of Green Chemistry & Chemical Processes, Department of Chemistry Wang, Yu-Xuan; East China Normal University, Shanghai Key Laboratory of Green Chemistry and Chemical Processes, Department of Chemistry Chen, Li-Jun; East China Normal University, Shanghai Key Labs of Green Chemistry & Chemical Processes, Department of Chemistry Yang, Hai-Bo; East China Normal University, Shanghai Key Labs of Green Chemistry & Chemical Processes, Department of Chemistry

SCHOLARONE™
Manuscripts

Chem Soc Rev

Dynamic Article Links ▶

TUTORIAL REVIEW

Construction of multiferrocenyl metallacycles and metallacages *via* coordination-driven self-assembly: From structure to functions

Lin Xu, Yu-Xuan Wang, Li-Jun Chen and Hai-Bo Yang*

Recently, the construction of discrete multiferrocenyl organometallic structures *via* coordination-driven self-assembly has attracted considerable attention because of their interesting electrochemical properties and wide applications in the areas of organometallic chemistry, electrochemistry, and materials science. Coordination-driven self-assembly has proven to be a simple yet highly efficient approach for the
10 preparation of various multiferrocenyl metallacycles and metallacages with predetermined shapes and sizes as well as the distribution and total number of ferrocenes. This review focuses on the recent progress in the construction of a variety of discrete multiferrocenyl metallacycles and metallacages *via* coordination-driven self-assembly. The characterization, the structure-related electrochemical properties, and the applications of these multiferrocenyl supramolecular architectures are also discussed.

15 1. Introduction

Ferrocene, as a specific and unique sandwich-type organometallic complex containing iron and two cyclopentadienide ligands, features the stable and readily oxidized properties, which allows for providing a facile scaffold for construction of various
20 ferrocenyl architectures with desired functions.[1] Since the discovery of ferrocene in 1951 by Kealy and Pauson,[2] ferrocene and its derivatives have attracted increasing interest in wide areas like electrochemistry, asymmetric catalysis, functional biomaterials, *etc*.[3] For instance, there has been an increasing use
25 of ferrocene derivatives as chiral auxiliaries in homogenous asymmetric catalysis not only in basic research bust also in industry.[4] In fact, owing to the extensive applications of ferrocene in organometallic chemistry, the discovery of ferrocene is generally considered as the starting point of modern
30 organometallic chemistry.

Over the past few decades, the design and synthesis of multiferrocenyl species has evolved to be one of the most attractive topics within organometallic chemistry because of their wide applications as multielectron reservoirs, elector-transfer
35 mediators, photochemical sensors, and building blocks for molecular electronic devices.[5] For example, Astruc *et al.* have successfully synthesized a new family of rigid hexakisferrocenyl star-shaped molecules **1** and **2** through Negishi coupling reaction and investigated their electron-transfer properties as well as the
40 implication of the electrostatic factor (Fig. 1).[6] However, to date, the most known multiferrocenyl complexes have been prepared as, or incorporated into, polymers or dendrimers, which often involve a tedious multistep methodology that requires considerable synthetic effort and sometimes is plagued by low
45 yields and largely amorphous final structures.[7] Furthermore, polymeric and dendritic macromolecules often possess large,
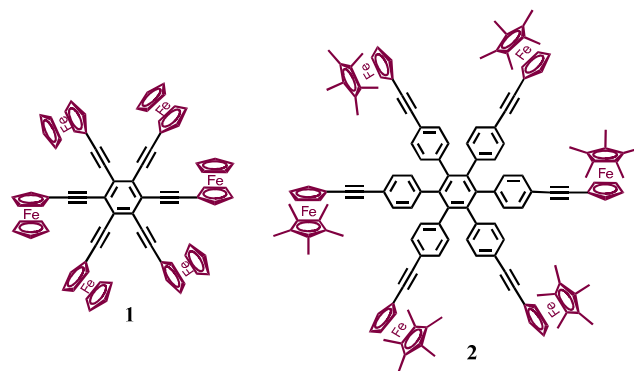

Fig. 1 The structures of hexakisferrocenyl star-shaped molecules **1** and **2**.

flexible, and/or globular structures that are not well-defined,
50 potentially limiting their further application in materials science. Therefore, the facile construction of multiferrocenyl architectures with precise control over the size and shape has been very challenging.

Coordination-driven self-assembly, which is based on metal–
55 ligand coordination interaction, has emerged as a powerful tool to construct discrete supramolecular two-dimensional (2-D) polygons and three-dimensional (3-D) polyhedra with considerable synthetic advantages including few steps, fast and facile construction of the final products, and inherent self-
60 correcting, defect-free assembly.[8] Over the past three decades, the groups of Lehn, Stang, Fujita, Mirkin, Raymond, and others have successfully employed the coordination-driven self-assembly strategy to build various of supramolecular polygons and polyhedra with well-defined geometry.[9] Generally, such synthesis
65 strategy based on coordination-driven self-assembly is straightforward and the yield is nearly quantitative. Moreover, coordination-driven self-assembly allows for the precise control over the shape and size of the final construction as well as the

distribution and total number of incorporated functional moieties such as ferrocene. The ability to fine tune the size, shape, distribution, and distance between electro-active ferrocenes would help provide a better understanding of the influence to

5 electrochemistry caused by the structural factors. Thus, during the past few years, a great number of various multiferrocenyl metallacycles and metallacages have been successfully constructed through coordination-driven self-assembly strategy.[10]

Although the design and synthesis of multiferrocenyl

10 organometallic atchitectures has evolved to be one of the most active and interesting areas in modern supramolecular chemistry and materials science, surprisingly, no review on the construction of discrete multiferrocenyl oranometallic complexes *via* coordination-driven self-assembly has been summarized to the

15 best of our knowledge. Considering the rapid development of this field, it is time to summarize the recent development of the construction of discrete multiferrocenyl organometallic architectures. In this review we will focus on the recent progress in the construction of discrete multiferrocenyl metallacycles and

20 metallacages *via* coordination-driven self-assembly. In addition, the characterization, electrochemical properties, and applications of representative multiferrocenyl complexes will be discussed as well.

2. Multiferrocenyl metallacycles

25 In general, there are four methods for incorporating functionalities into the discrete organometallic polygons.[8] Firstly, through the introduction of a functional moiety onto the exterior surface of a directional building block, an *exo*-functionalized metallacycles can be prepared. Secondly, a functional moiety

30 could be attached into the "inside" of a directional building block with a turning angle less than 180°, which allows for the formation of an *endo*-functionalized supramolecular metallacycle. In addition, a functional moiety can be incorporated as the edge or corner of a building block to construct an *edge*- or *corner*-

35 functionalized self-assembly. It should be noted that, different from the *exo*- or *endo*-functionalized metallacycles, the introduced functional moiety in the *edge*- or *corner*-functionalized multiferrocenyl architectures should be the part of the main backbone of the resultant metallacycles. Therefore, the

40 construction of four different types of muliferrocenyl metallacycles was summarized accordingly.

2.1 *Exo*-functionalized multiferrocenyl metallacycles

According to the "directional bonding" and "symmetry interaction" models, the shape of an individual 2D polygon is

45 usually determined by the value of the turning angle within its angular components. For example, the combination of the 120° unit with the complementary 60° linking components will yield a molecular rhomboid.[8] Recently, Stang and White *et al.* synthesized a ferrocenyl 120° donor building block **3** attached

50 with a ferrocenyl group on the periphery *via* a coupling reaction of ferrocene-1-carboxylic acid and 3,5-bis-(pyridin-4-ylethynl)phenol (Fig. 2).[10] Stirring the mixture of **3** and complementary 60° di-Pt(II) acceptor **4** in a 1:1 stoichiometric ratio for 12 h, the bisferrocenyl rhomboid **5** with pendant

55 ferrocene groups at donor vertex was prepared in excellent yields (97%) through coordination-driven self-assembly, thus avoiding
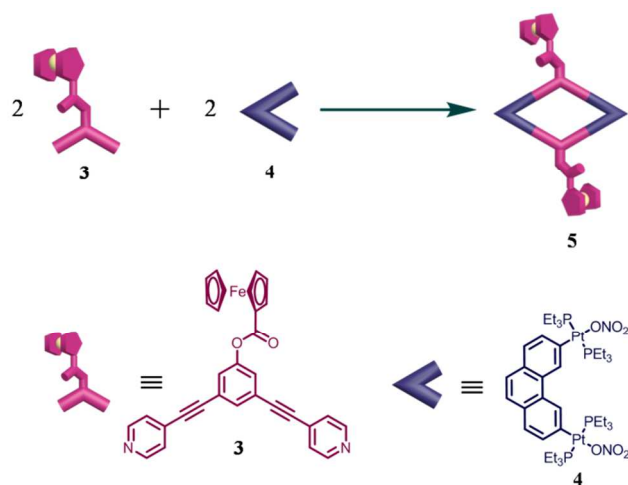

Fig. 2 Cartoon representation of the formation of bisferrocenyl rhomboid **5** from 120° donor **3** and 60° acceptor **4**.
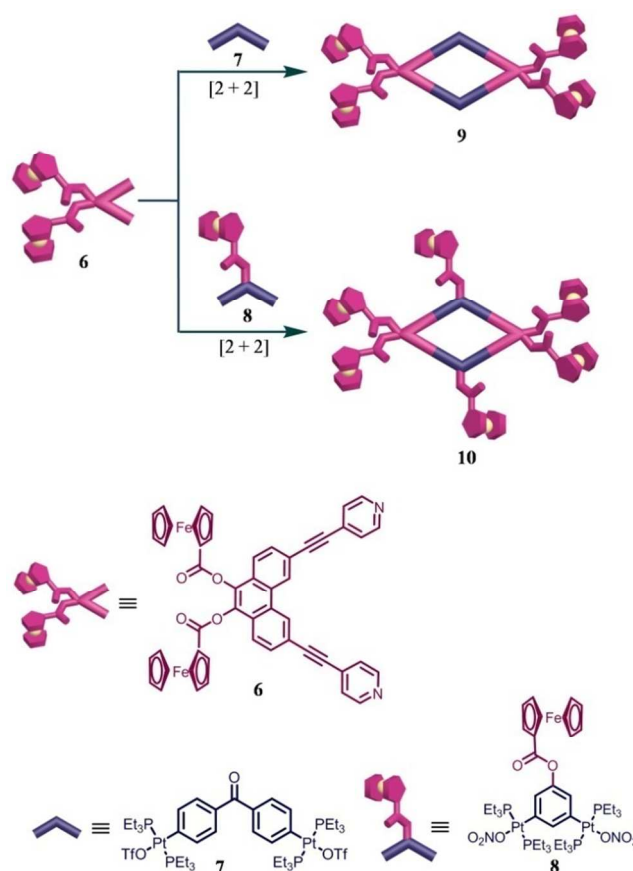

60 **Fig. 3** Cartoon representation of the formation of tetrakisferrocenyl rhomboid **9** and hexakisferrocenyl rhomboid **10** from 60° donor **6** and 120° acceptor **7** or **8**, respectively.

the time-consuming procedures and low yields that often

65 encountered in covalent synthesis protocols.

With the aim to developing new multiferrocenyl rhomboids, Yang *et al.* synthesized a ferrocenyl 60° donor **6** attached with two ferrocene groups on the periphery, from which the tetrakisferrocenyl rhomboid **9** and hexakisferrocenyl rhomboid **10**

70 were prepared by mixing the 60° donor **6** with 120° acceptor **7** or **8** in a 1:1 stoichiometric ratio at room temperature *via*

coordination-driven self-assembly, respectively (Fig. 3).[11]

The structures of the multiferrocenyl rhomboids **5**, **9**, and **10** were confirmed by multinuclear NMR {^{1}H and ^{31}P} spectroscopy and mass spectrometry (electrospray ionization mass
[5] spectrometry (ESI-MS) or cold-spray ionization time-of-flight mass spectrometry (CSI-TOF-MS)). The analysis of NMR spectra revealed the formation of discrete, highly symmetric multiferrocenyl rhomboids. For example, the ^{31}P {^{1}H} NMR spectra of **5**, **9**, and **10** displayed a sharp singlet (*ca.* 12.2 ppm for
[10] **5**, 13.3 ppm for **9**, and 16.1 ppm for **10**) shifted upfield from the precursors **4**, **7**, and **8** by approximately 11.8 ppm, 6.7 ppm, and 3.8 ppm, respectively. This change, as well as the decrease in the coupling of the flanking ^{195}Pt satellites, was consistent with back-donation from the platinum atoms. In the ^{1}H NMR spectrum of
[15] each assembly, the hydrogen nuclei of the pyridine rings exhibited downfield shifts because of the loss of electron density that occurred upon coordination of the pyridine-N atom with the Pt(II) metal center. Additionally, the structures of the rhomboidal metallacycles **5**, **9**, and **10** were further confirmed by mass
[20] spectrometry (ESI-MS or CSI-TOF-MS). For instance, the ESI mass spectrum of **5** showed a peak at *m/z* = 1609.2, corresponding to the charge state resulted from the loss of two nitrate counterions $[M - 2NO_3]^{2+}$, where M represents the intact assembly. The peak was isotopically resolved and agreed well
[25] with the theoretical distribution. Molecular force-field simulations revealed that **5** featured a well-defined rhombus with an approximately 2.4 × 1.6 nm cavity, while **9** and **10** featured the similar planar rhombus structures yet the larger sized cavities (2.9 × 2.0 nm for **9** and 2.7 × 1.7 nm for **10**).
[30] Interestingly, the electrochemical studies of **5**, **9**, and **10** disclosed that their electrochemical behaviour was somewhat different although they featured the similar rhombus scaffold. For instance, rhomboid **5** showed stable and independent electrochemically active and exhibited one-electron reaction
[35] responses. However, rhomboids **9** and **10** displayed distorted and merged cathodic and anodic waves in cyclic voltammetry (CV) investigations, which indicated that the electronic communication existed between two ferrocenyl groups attached on phenanthrene. This finding was further supported by the simulated molecular
[40] models that revealed the distance between two Fe atoms being about 0.8 nm, thus making the Coulombic interaction possible. Moreover, due to the presence of two types of ferrocenyl groups in the assembly, rhomboid **10** showed much more complicated electrochemical behavior than that of **9**.
[45] Since the first example of an organogold molecular triangle reported by Vaughan in 1970, the construction of triangle metallacycles has attracted much attention.[12] However, the formation of discrete triangles sometimes suffers from the noticeable equilibrium with other macrocyclic species,
[50] particularly when flexible building blocks are employed. In order to overcome this problem, the rigid 60° ditopic tecton based on phenanthrene skeleton was employed by Stang *et al*, from which a series of well-defined supramolecular triangles were formed when combined with three linear bidentate ligands through
[55] coordination-driven self-assembly, respectively.[13] Based on this strategy, Yang *et al.* prepared a family of novel hexakisferrocenyl triangles **15–17** *via* [3 + 3] coordination-driven self-assembly by heating the mixture of 60° ferrocenyl diplatinum acceptor **11** and
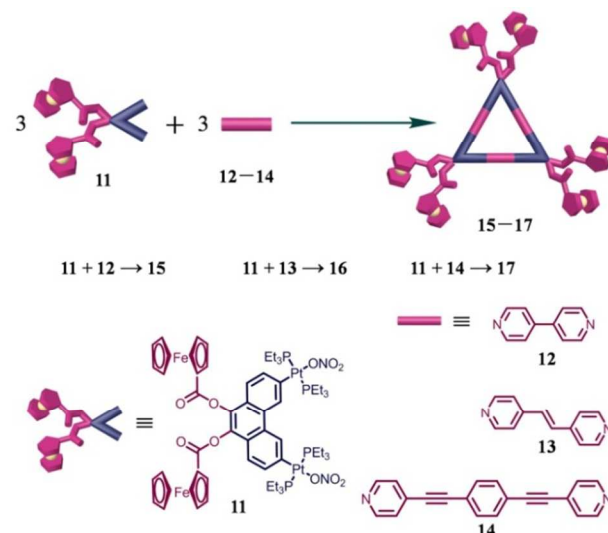

[60] **Fig. 4** Cartoon representation of the formation of hexakisferrocenyl triangles **15–17** from 60° acceptor **11** and 180° donors **12–14**, respectively.
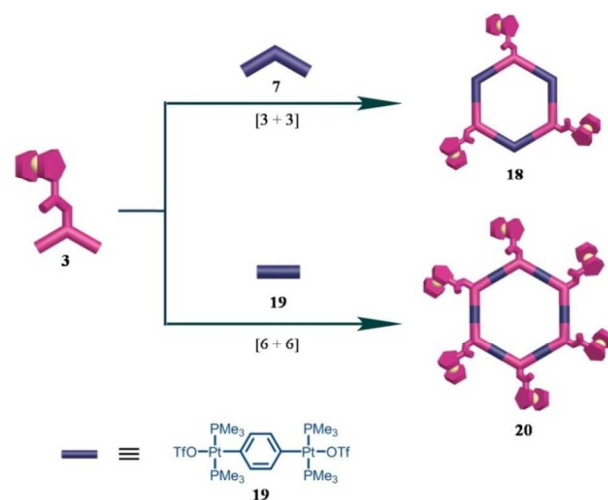

Fig. 5 Cartoon representation of the formation of trisferrocenyl hexagon
[65] **18** and hexakisferrocenyl hexagon **20** from 120° donor **3** and 120° acceptor **7** or 180° acceptor **19**, respectively.

the linear donors **12–14** with different lengths in a 1 : 1 stoichiometric ratio in aqueous acetone (1/1, v/v, water/acetone) overnight, respectively (Fig. 4).[14] Due to the different lengths of
[70] the linear building blocks **12–14** employed in the self-assembly, PM6 semiempirical molecular orbital studies revealed that the final hexakisferrocenyl triangles **15–17** featured different sizes. The sides of the triangles **15–17** were found to be 4.0, 4.2, and 5.0 nm in length, respectively.
[75] Similar to rhomboidal complexes **9** and **10**, triangles **15–17** showed distorted and merged cathodic and anodic waves in CV investigation, which might be caused by the electronic communication between two ferrocenyl groups attached on the phenanthrene. Moreover, the electrochemical studies indicated
[80] that the ratio of diffusion coefficient (*D*) of **15**, **16**, and **17** was 1.37 : 1.36 : 1.0, which was consistent with an inverse ratio of outer diameters of 4.0, 4.2, and 5.0 nm for **15**, **16**, and **17** obtained from molecular modelling, since *D* is inversely proportional to the molecular size.
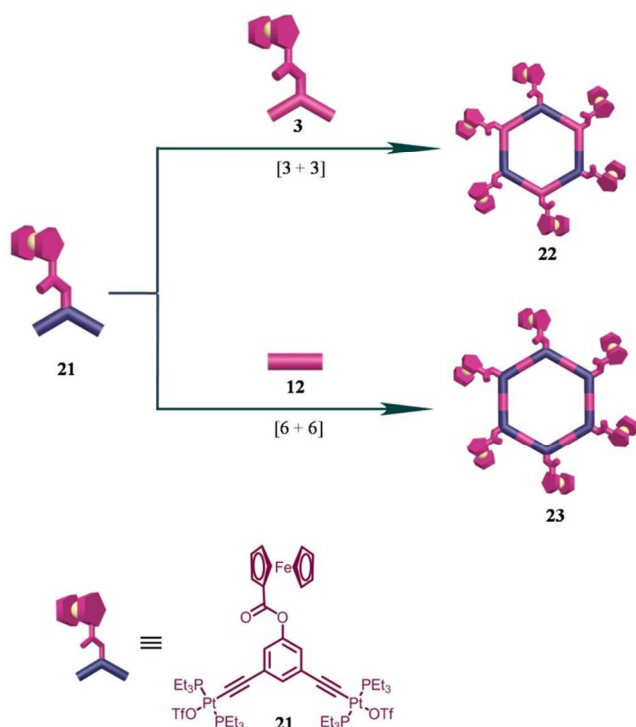
Fig. 6 Cartoon representation of the formation of hexakisferrocenyl hexagons **22** and **23** from 120° acceptor **21** and 120° donor **3** or 180° donor **12**, respectively.

According to the "directional bonding" and "symmetry interaction" models, hexagonal metallacycle could be prepared from the combination of two complementary ditopic building block, each incorporating 120° angles between the active coordination sites as well as the combination of six 120° building blocks with six appropriate linear linker units.[9] Recently, Stang and White *et al.* reported the construction of [3 + 3] trisferrocenyl hexagon **18** and [6 + 6] hexakisferrocenyl hexagon **20** through the interaction of the 120° donor **3** with an equimolar amount of 120° di-Pt(II) acceptor **7** or the linear acceptor **19** at room temperature, respectively (Fig. 5).[10]

Another series of hexakisferrocenyl hexagons were prepared from the ferrocenyl 120° di-Pt(II) acceptor **21** *via* two approaches reported by Stang and co-worker.[15] For example, as shown in Fig. 6, they prepared [3 + 3] hexakisferrocenyl hexagon **22** through the reaction of the ferrocenyl 120° di-Pt(II) acceptor **21** with an equimolar amount of the ferrocenyl 120° donor **3**. Furthermore, stirring **21** with an equimolar amount of the linear donor **12** in CD_2Cl_2 at room temperature resulted in the formation of [6 + 6] hexakisferrocenyl hexagon **23** in excellent yield (> 96%).

The molecular force-field simulations revealed very similar planar hexagonal structures for **18**, **20**, **22**, and **23**, yet different sized cavities with the sequence of **22** < **18** < **23** < **20**. The above study provided a simple yet highly efficient approach to the construction of *exo*-derivatized hexagons containing well-defined cavities of varying diameters and number of ferrocenes *via* coordination-driven self-assembly.

The cyclic voltammograms of all hexagons **18**, **20**, **22**, and **23**, obtained at various scan rates, showed cathodic/anodic peak current ratios of $i_c/i_a \approx 1$, indicating that all of the oxidized complexes were chemically stable on the voltammetric time scale
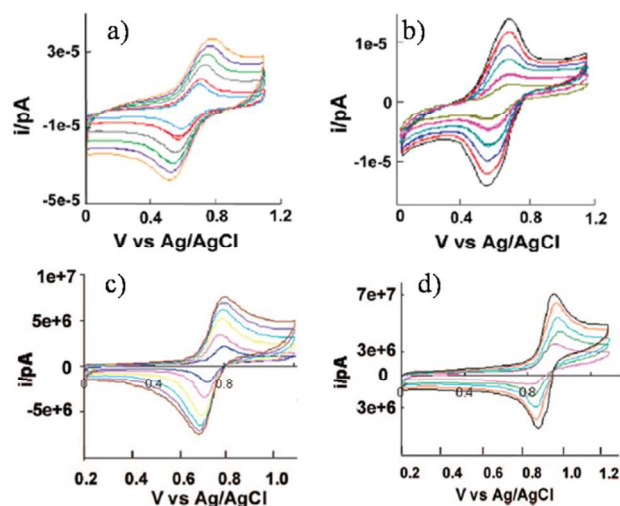

Fig. 7 Cyclic voltammograms of 0.20 mM **18** (a), 0.21 mM **20** (b), 0.20 mM **22** (c), and 0.20 mM **23** (d) at a scan rate of 25-250 mV/s. Copyright 2008 American Chemical Society.

(Fig. 7). Interestingly, the electrochemical studies revealed that there was an increase in their half-wave potentials ($E_{1/2}$) of **22** and **23** with the increase of the sizes, however, the half-wave potentials ($E_{1/2}$) of **18** and **20** decreased with the increase of the sizes.

In addition to being a successful methodology to construct *homo*-functional supramolecular polygons, the coordination-driven self-assembly strategy has proven to be a readily and efficient strategy to construct *hetero*-functional metallacycles through the combination of complementary precursors substituted with different functional moieties.[8] It should be noted that the incorporation of different functional moieties into metallacycles generally endows them with versatile properties.

Since the pioneering work by Newkome and co-workers in the early 1990s,[16] the construction of supramolecular metallodendrimers has evolved to be one of the most attractive fields within dendrimer chemistry due to their wide applications such as catalysts, supramolecular redox sensors, biological mimetics, and light-harvesting antennae, *etc.* Recently, Yang *et al.* constructed a series of dendritic ferrocenyl metallacycles. For example, the dendritic bisferrocenyl rhomboids **25a–c** were prepared by stirring the mixture of 120° ferrocenyl di-Pt(II) acceptor **8** with an equimolar amount of 60° dipyridyl donors **24a–c** substituted with Fréchet type dendrons, respectively (Fig. 8).[17] In order to extend the investigation to the construction of dendritic multiferrocenyl rhomboids, Yang *et al.* prepared another series of [2 + 2] dendritic tetrakisferrocenyl rhomboids **27a–c**[18] and [3 + 3] dendritic trisferrocenyl hexagons **28a–c**[19] through the combination of 120° [G1]–[G3] dendritic dipyridyl donors **26a–c** and 60° bisferrocenyl acceptor **11** or 120° ferrocenyl acceptor **21**, respectively (Fig. 9).

In the above-mentioned examples, the square planar platinum metal was explored to connect with nitrogen-based organic building blocks such as the substituted pyridines. Thus the resulting supramolecular metallodendrimers were positively charged, bearing as many positive charges as Pt–N coordination bonds. Recent research indicated that neutral organometallic
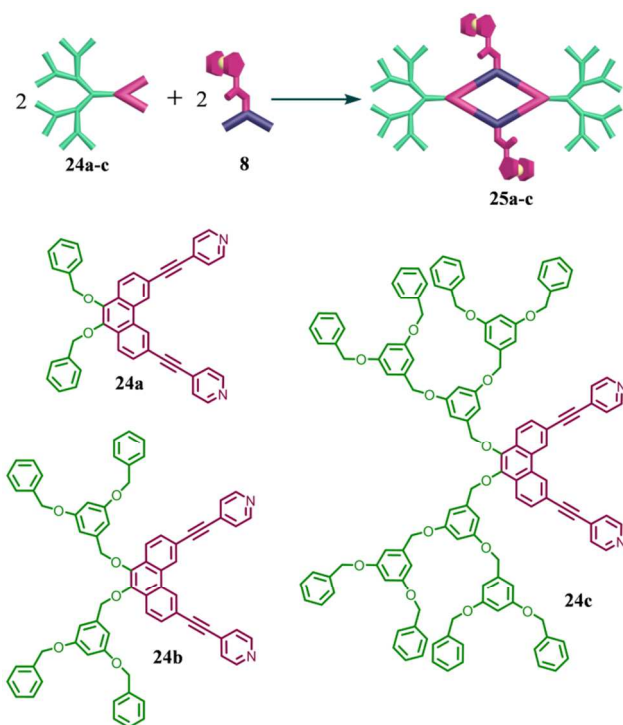
Fig. 8 Cartoon representation of the formation of dendritic bisferrocenyl rhomboids **25a–c** from 60° [G1]–[G3] dendritic donors **24a–c** and 120° acceptor **8**, respectively.

supramolecular structures featured some advantages. For example, they are more readily soluble in organic solvents and are likely to be more suitable for the encapsulation of neutral organic guests.[20] Along similar lines as those used to prepare the charged dendritic multiferrocenyl metallacycles **27a–c** and **28a–c**, additional examples of neutral dendritic tetrakisferrocenyl rhomboids **30a–c**[18] and trisferrocenyl hexagons **31a–c**[21] were also prepared by Yang *et al.* based on platinum–oxygen (Pt-O) coordination bonds through the combination of 120° dicarboxylate donors **29a–c** with 60° bisferrocenyl di-Pt(II) acceptor **11** or 120° ferrocenyl di-Pt(II) acceptor **8**, respectively (Fig. 9).

It should be noted that the $^{31}P\{^1H\}$ NMR spectra of the neutral assemblies **30a–c** and **31a–c** displayed a sharp singlet shifted upfield from their corresponding starting platinum acceptor **11** and **8** by approximately 2.0 ppm and 1.8 ppm, respectively. In comparison to their corresponding charged assemblies **27a–c** and **28a–c**, where the corresponding shifts were *ca.* 7.0 ppm and 6.0 ppm, the shifts were noticeably smaller. These smaller shifts could be attributed to the similarity between the newly formed platinum–oxygen bond and the Pt–ONO$_2$ bond in the starting platinum acceptors. The CV investigation revealed that the neutral dendritic metallacycles exhibited the similar electrochemical behavior to their corresponding charged assemblies. For instance, all dendritic metallacycles showed one-electron reaction response. Moreover, the *D* values were found to decrease along with an increase of the generation of dendritic metallacycles.

Crown ethers and their structural analogues have developed to be a family of classical covalent macrocycles that played an important role in host–guest chemistry and the construction of structurally interesting molecular architectures since the
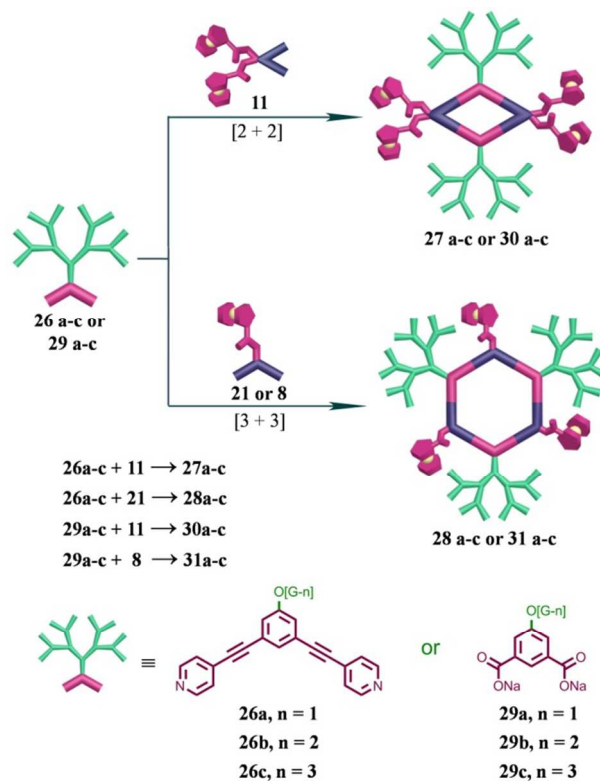

Fig. 9 Cartoon representation of the formation of dendritic tetrakisferrocenyl rhomboids **27a–c** and **30a–c** and dendritic trisferrocenyl hexagons **28a–c** and **31a–c**.
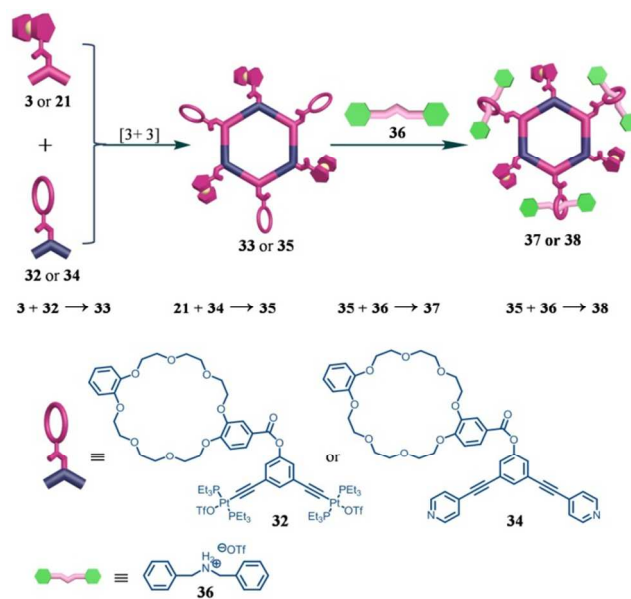

Fig. 10 Cartoon representation of the formation of hetero-functional hexagons **33**, **35**, **37**, and **38**.

discovery of crown ether by Pedersen in 1967.[22] During the last two decades, steadily growing research interest has been devoted to the design of multiple crown ether derivatives, which can be used in multicomponent host–guest recognition or in the construction of higher order complexes.[23] Stang and White *et al.* prepared a *hetero*-functional hexagon **33** by stirring the mixture of 120° ferrocenyl donor unit **3** and 120° crown ether

functionalized building block **32** in CH$_2$Cl$_2$ for 30 minutes at room temperature.[24] In a complementary manner, stirring 120° ferrocenyl acceptor **21** with an equimolar amount of 120° crown ether donor **34** in CH$_2$Cl$_2$ resulted in the formation of *hetero*-functional hexagon **35** (Fig. 10).

The electrochemical studies of **33** and **35** showed that the oxidation of the ferrocene moieties in each complex was chemically reversible and each ferrocene group was oxidized independently. Moreover, the presence of the crown ether did not have any influence on the electrochemical properties of the ferrocenyl units. In order to study the effect of the binding of crown ether units with dibenzylammonium triflate salt **36** to the electrochemical properties of **33** and **35**, investigation of the self-assembly of tris[2]pseudorotaxanes was carried out. Upon adding 3.0 equiv. of **36** to a solution of hexagonal metallacycle **33** or **35** within 15 minutes, respectively, tris[2]pseudorotaxane **37** or **38** was obtained. Cyclic voltametric studies of pseudorotaxanes **37** and **38** showed no significant change in $E_{1/2}$ after binding the ammonium salts, indicating that the crown ether and ferrocene moieties were noninteracting. Nevertheless, the absolute currents of the voltammetric waves were both slightly decreased for **37** and **38**, as compared to that of **33** and **35**, respectively, which might be attributed to the larger sizes and higher charges of **37** and **38** compared to **33** and **35**.

2.2 *Endo*-functionalized multiferrocenyl metallacycles

Compared to many reports on the construction of multiferrocenyl metallacycles *via* *exo*-functionalization strategy, there were rare reports on the synthesis of *endo*-functionalized ferrocenyl metallacycles. Recently, Yang *et al.* constructed a new family of multiferrocenyl hexagons **40** and **41** through *endo*-functionalized approach *via* coordination-driven self-assembly by mixing a 120° *endo*-ferrocenyl donor ligand **39** with 120° acceptor **7** or 180° di-Pt(II) acceptor **19** in a 1:1 ratio, respectively (Fig. 11).[25] The molecular modelling revealed that the [6 + 6] hexagon **41** had a larger internal radius of 3.3 nm than that of the [3 + 3] hexagon **40** (*ca.* 2.2 nm). Additionally, it was found that the distance between the nearest two ferrocenyl units was approximately 1.4 nm for **40** and 1.7 nm for **41**, respectively, which exceeded the distance for the possible interaction between two ferrocene subunits.
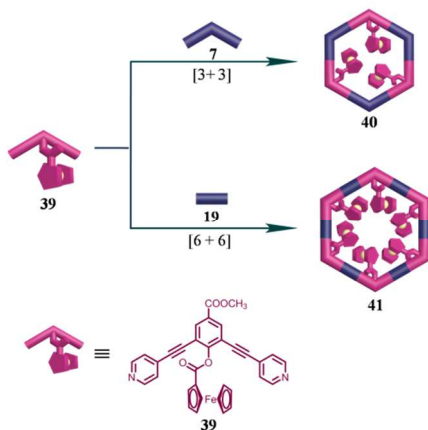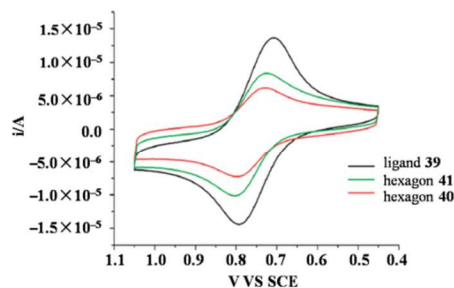

Fig. 12 Cyclic voltammetrys of 0.2 mM solution of ligand **39** and multiferrocenyl hexagons **40** and **41**. Copyright 2012 American Chemical Society.

Different from the previous reports on the electrochemical behavior of *exo*-functionalized multiferrocenyl metallacycles, the cyclic voltammetry investigation demonstrated that assemblies **40** and **41** featured a 15 and 23 mV positive shifts relative to ligand **39**, respectively (Fig. 12). In other words, hexagons **40** and **41** were more difficult to be oxidized, which might be caused by the loss of electron density upon coordination of the nitrogen lone pair to the platinum metal centers. Additionally, the peak current of ligand **39** was larger than that of trisferrocenyl hexagon **40** and hexakisferrocenyl hexagon **41**, although two hexagons possessed more electro-active ferrocene sites under the same conditions. All ferrocenyl units of *endo*-functionalized multiferrocenyl hexagons were located in the inner surface of the metallacycles, which made it difficult to access to the electrode, thus resulted in the lower magnitude of the current. The results indicated that the environment featured a non-negligible influence on electrochemical behaviour when ferrocene groups incorporated into the interior surface of supramolecular metallacycles.

Recently, Würthner *et al.* synthesized a series of ferrocenyl-substituted squares **44a-b**, in which sixteen ferrocene units were introduced into the square scaffold (Fig. 13).[26] By mixing the ferrocene-substituted linear donors **42a**–**b** with an equimolar amount of 90° acceptor [Pt(1,3-bis(diphenylphosphino) propane)][(OTf)$_2$] **43** in dichloromethane at room temperature resulted in the formation of multiple ferrocenyl squares **44a**–**b**.

Interestingly, the investigation of the electrochemical behaviour of ligand **42a** and the corresponding metallacycle **44a** pinpointed a supramolecular effect on their electrochemical properties. For instance, the cyclic voltammogram of square **44a**

Fig. 11 Cartoon representation of the formation of multiferrocenyl hexagons **40** and **41** from 120° donor **39** and 120° acceptor **7** or 180° acceptor **19**, respectively.
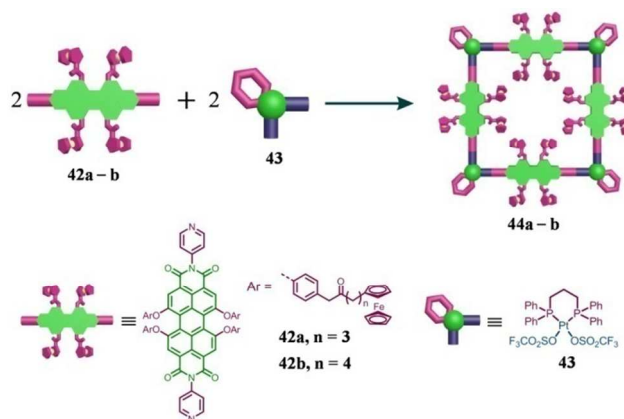

Fig. 13 Cartoon representation of the formation of squares **44a-b** from linear donors **42a-b** and 90° acceptor **43**, respectively.
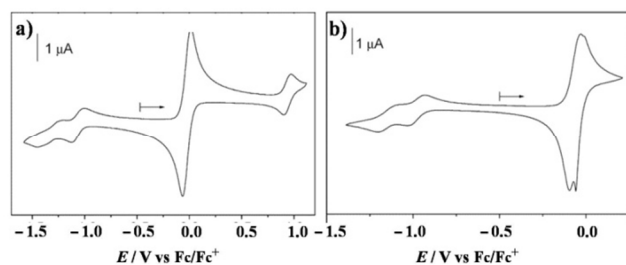
Fig. 14 Cyclic voltammograms of ligand **42a** (a) and metallacycle **44a** (b) in CH_2Cl_2, sweep rate 100 mVs^{-1}. Copyright 2003 American Chemical Society.
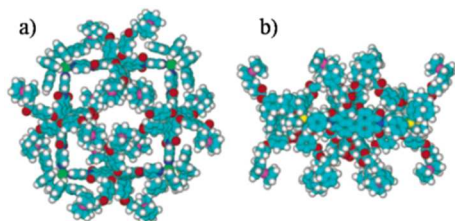

Fig. 15 Top (a) and side (b) views of energy minimized structures of molecular square **44a**. Copyright 2003 American Chemical Society.

showed peaks splitting at $E = -0.06$ and -0.10 V for the reductive wave and at $E = -0.03$ V and a shoulder at $E = -0.01$ V for the oxidative wave (Fig. 14). However, such a peak splitting was not observed in the case of the free ligand **42a**. The square **44b** exhibited the similar electrochemical behaviour with **44a**.

In order to understand the observed supramolecular effect on the reduction process of ferrocenium groups, the pertinent structural features of squares **44a**–**b** characterized by X-ray analysis and molecular modeling were investigated as well. When ligand **42a** or **42b** was self-assembled into a square scaffold, the twisted structures were observed, in which sixteen ferrocene units were separated into two groups. One set was pointed toward the inside of the square cavity while the other set oriented outside of the square cavity. Indeed, molecular dynamic simulation of square **44a** confirmed these structural features (Fig. 15). However, the ferrocenium moieties inside the square were located in a more hydrophobic microenvironment than that of the outside ferrocenium groups. Thus, the outside ferroceniums were stabilized by the bulky polar electrolyte, while the inside ferroceniums were not easily accessible by the polar electrolyte, thus being less stable. Consequently, the inside ferroceniums were more easily reduced to ferrocene than the outside ones, *i.e.*, exhibiting a higher $E_{1/2}$ value. Therefore, two peaks were observed in the reduction cycle of ferroceniums in the cyclic voltammograms of square **44**. This study demonstrated that the redox properties of these sixteen ferrocenyl subunits were strongly affected by the sterical constraint imposed by the core square superstructure.

2.3 *Edge*-functionalized multiferrocenyl metallacycles

Ferrocene features a unique ring scaffold with relative rigidity. In addition, the cyclopentadienyl ring in ferrocene carries a partial negative charge, which allows it to be derivatized easily. Therefore, ferrocene has evolved to be a suitable scaffold for designing new building blocks for further self-assembly. In general, 1,1'-disubstituted ferrocenyl ligands, including *syn*-1,1'-
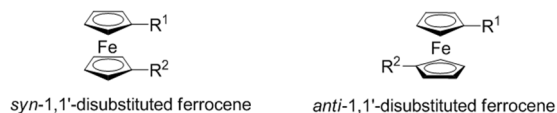

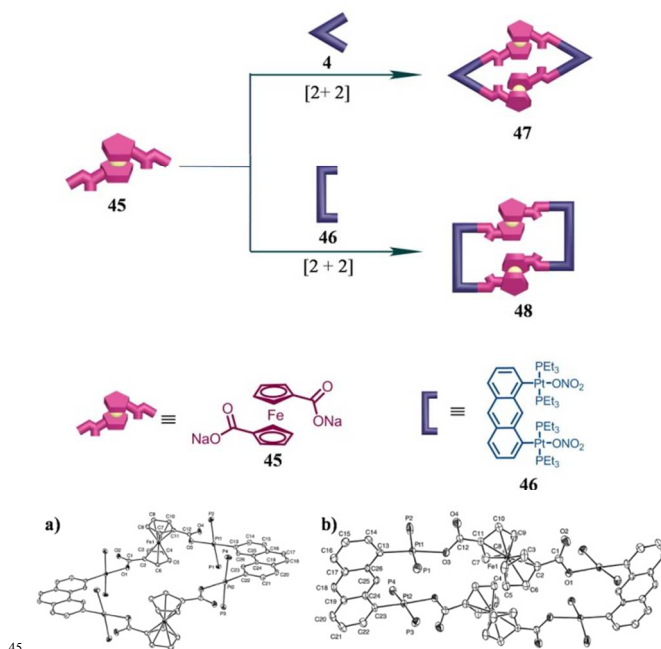**Fig. 16** The two types of 1,1'-disubstituted ferrocene ligand.

Fig. 17 Cartoon representation of the formation of bisferrocenyl rhomboid **47** and rectangle **48** from donor **45** and 60° acceptor **4** or 0° acceptor **46**, respectively; the crystal structures of **47** (a) and **48** (b).

disubstituted ferrocene complex and *anti*-1,1'-disubstituted ferrocene derivative, have been extensively utilized in coordination-driven self-assembly (Fig. 16). Different from the *exo*- or *endo*-functionalized multiferrocenyl metallacycles, the 1,1'-disubstituted ferrocenyl ligand in *edge*-functionalized multiferrocenyl architectures is part of the backbone of the resultant metallacycle, which may endow the final architecture interesting electrochemical properties.

Stang *et al.* synthesized a dicarboxylate ligand, 1,1'-ferrocenedicarboxylic acid **45** (Fig. 17).[27] Interestingly, unlike other aromatic dicarboxylates, **45** is a more flexible linker with various geometries under different coordinating modes. For instance, stirring **45** with an equimolar amount of 60° acceptor **4** or 0° acceptor **46** resulted in the formation of neutral bisferrocenyl rhomboid **47** or rectangle **48** in 95% yield, respectively.[27] X-ray crystallographic analysis of **47** and **48** provided the unambiguous support for the existence of such neutral bisferrocenyl metallacycles based on Pt-O bonds (Fig. 17). Further analysis revealed that **47** featured a rhombus with a 14 × 20 Å cavity, while **48** featured a rectangle with a 18 × 6 Å cavity. Moreover, the coordination mode of the dicarboxylate groups in both **47** and **48** was *syn-syn* and the torsion angle for the two Cp rings was *ca.* 156° for **47** and 146° for **48**, respectively. Cyclic voltammetry of metallacycle **48** in dichloromethane displayed two oxidation waves, each corresponding to a double one-electron transfer from the two equivalent ferrocenes and anthracene bridges. The cathodic counter peaks were separated from the corresponding anodic

oxidation peaks by about 60 mV. Metallacycle **48** was found to be the first example with two different kinds of reversibly *oxidizable* sides of a molecular rectangle that could be reversibly oxidized in two two-electron steps.

5   Duan and Meng *et al.* prepared a tetrakisferrocenyl metallacycle **50** by stirring the mixture of ferrocene-bridged bis-tridentate ligand **49** with Ni(BF$_4$)$_2$ and NaOH in a 1:1:2 molar ratio in methanol at boiling temperature (Fig. 18).[28] The structure of **50** was unequivocally confirmed by ESI-MS spectrometry and 10 X-ray crystallographic study. The differential pulse voltammetry (DPV) of metallacycle **50** showed a single-electron Fe^{III}/Fe^{II} couple oxidation process with half-wave potential ($E_{1/2}$) at 1.02 V. Interestingly, the addition of 2.0 equiv of Mg(NO$_3$)$_2$ to the solution of metallacycle **50** induced a clear evolution of the 15 voltammogram (Fig. 19). Moreover, the redox peak of the Fe^{III}/Fe^{II} couple was found to shift to 0.78 V. However, under the identical conditions, the addition of some other nitrate salts, such as LiNO$_3$, NaNO$_3$, KNO$_3$, Ba(NO$_3$)$_2$, and Ca(NO$_3$)$_2$, resulted in a negligible change in voltammogram. The voltammogram 20 evolution of **50** responding to Mg^{2+} suggested that Mg^{2+} might be captured by the oxygen atoms coordinated to the long diagonal nickel atoms. It should be noted that, in general, the addition of a metal cation into the sensor compounds will induce a classical anodic shift of the iron potential, however, the opposite result was 25 observed in the case of complex **50**.

    The investigation of anion recognition and sensing has received the rising interest within supramolecular chemistry recently.[29] However, the design and synthesis of novel host structures for highly efficient anion recognition is still very 30 challenging. Yu *et al.* realized the construction of bisferrocenyl
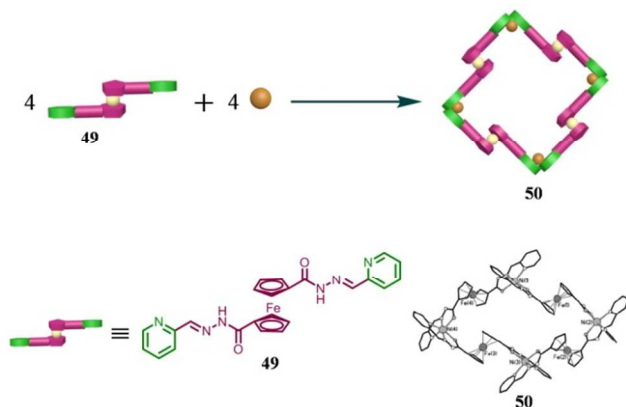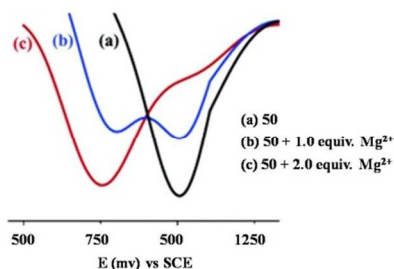

Fig. 18 Cartoon representation of the formation of tetrakisferrocenyl metallacycle **50** from **49**, Ni(BF$_4$)$_2$, and NaOH; the crystal structure of **50**.

35 **Fig. 19** Differential pulse voltammetrys for tetrakisferrocenyl metallacycle **50** in the absence (a) and presence of Mg^{2+} (1.0 equivalent (b), 2.0 equivalents (c)). Copyright 2004 American Chemical Society.
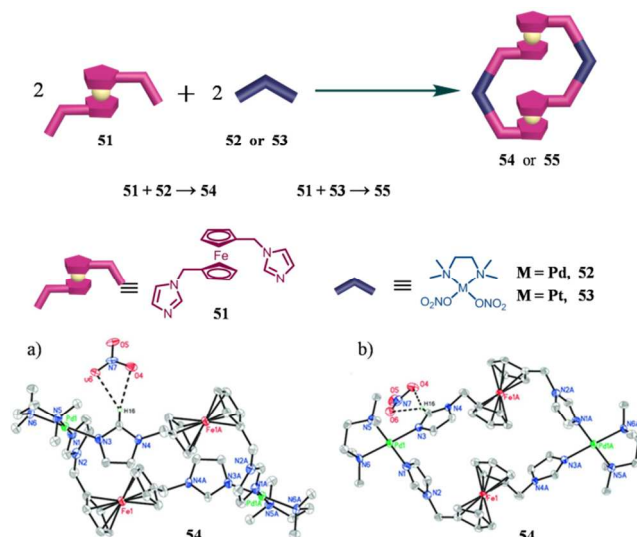

Fig. 20 Cartoon representation of the formation of bisferrocenyl 40 metallacycles **54** and **55** from donor **51** and acceptor **52** or **53**, respectively; the crystal structures of **54**, (a) side view; (b) top view. Thermal ellipsoids are shown at the 30% probability level.

metallacycles **54** and **55** that were capable of binding and recognizing anions from a flexible diimidazole ligand with 45 ferrocene as spacer.[30] For instance, as shown in Fig. 20, simply stirring the mixture of ligand **51** with an equimolar amount of (tetramethylethylenediamine)Pd(NO$_3$)$_2$ **52** in H$_2$O at room temperature over 12 h resulted in the formation of bisferrocenyl metallacycles **54**. The structure of **54** was unequivocally 50 confirmed by X-ray crystallography (Fig. 20). The X-ray crystallographic analysis revealed that the four cyclopentadiene rings of ferrocenes were parallel to each other. Furthermore, the dihedral angle between the two imidazole (N3–N4 and N2–N1) planes at each corner was found to be 78.9°.

55   The anion-sensing behaviour of bisferrocenyl metallacycle **54a** (the PF$_6^-$ salt of **54** that was obtained through anion exchange with 10-fold excess NH$_4$PF$_6$ in a methanol solution) was investigated by CV and square-wave voltammetry (SWV). As shown in Fig. 21, compared to NO$_3^-$, H$_2$PO$_4^-$, AcO$^-$, and F$^-$, the 60 addition of HSO$_4^-$ led to the most obvious change of the Ep values, which indicated that HSO$_4^-$ had the strong interaction with the redox center. Furthermore, the addition of HSO$_4^-$ induced a second wave with the more negative potential appeared, which might be attributed to the formation of a receptor–anion 65 complex. The CV titrations of HSO$_4^-$ to the CH$_3$CN solution of receptor **54a** provided the further support for the formation of
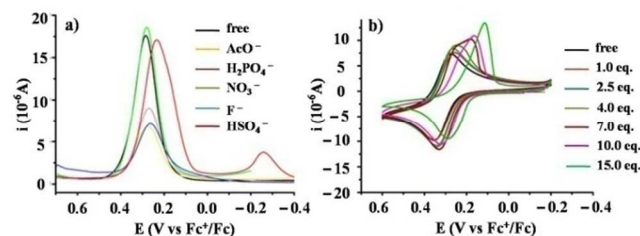

Fig. 21 (a) Evolution of the SWV of bisferrocenyl metallacycle **54a** in CH$_3$CN upon the addition of various anions (4 equiv). (b) CV of 70 bisferrocenyl metallacycle **54a** in CH$_3$CN upon the addition of various concentrations of HSO$_4^-$. Copyright 2011 American Chemical Society.
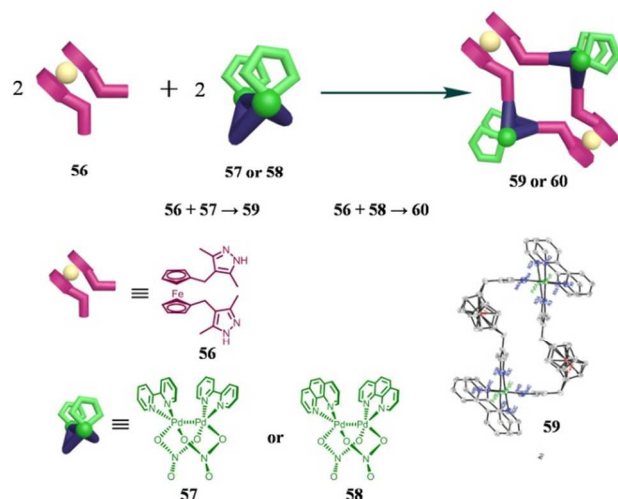
Fig. 22 Cartoon representation of the formation of multiferrocenyl metallacycles **59** and **60** from donor **56** and acceptor **57** or **58**, respectively; the crystal structure of **59**.

receptor–anion complex. Thus, bisferrocenyl metallacycle **54a** was capable of being utilized in anion recognition and sensing in aqueous solution.

Similar to the preparation of **54** and **55**, Yu *et al.* prepared a series of multiferrocenyl metallacycles **59** and **60** through the reaction of ferrocene-containing dipyrazole ligand **56** with dimetal corners [(2, 2′-bipyridine)$_2$Pd$_2$(NO$_3$)$_2$](NO$_3$)$_2$ **57** or [(1,10-phenanthroline)$_2$Pd$_2$(NO$_3$)$_2$](NO$_3$)$_2$ **58** *via* coordination-driven self-assembly, respectively (Fig. 22).[31] The structure of **59** was confirmed by X-ray crystallographic analysis, which revealed that the size of its inner square-shaped cavity was approximately 6×11 Å (Fig. 22). CV and SWV were employed to investigate the anion sensing properties of metallacycle **59**. It was found that the metallacycle **59** featured the good selectivity for Br$^-$ recognition. ^{1}H NMR spectroscopy studies revealed that the selective sensing of **59** for Br$^-$ was attributed to the formation of a new receptor–anion complex ([**59**·4Br]) by trapping four Br$^-$ *via* C–H···Br hydrogen bonds.

Porphyrin and its derivatives usually provide the rigid frameworks and feature a replaceable central metal ion, to which one or two axial basic ligands could coordinate. Recently, ferrocene-appended porphyrins have displayed potential applications in molecular electronic devices or as models for multiple-electron transfer reactions. Kobuke *et al.* prepared a ferrocene-bridged porphyrin trimer **61** decorated with imidazole groups at both ends of the terminal porphyrin (Fig. 23).[32] Because of the large association constant of imidazole and porphyrinatozinc(II) (more than 10^{11} M^{-1}), treatment of **61** with a methanol solution of Zn(II) acetate resulted in the formation of metallacycle **62**.

Since the obtained metallacycle **62** possessed two additional coordination sites available at the central Zn(II) porphyrin, the coordination behaviour of metallacycle **62** and the bidentate ligands with different spacer length was investigated by UV-vis titration (Fig. 24). For example, the addition of guest molecule 1,5-di(1H-imidazol-1-yl)pentane (**63**) induced a clear spectral change with an isosbestic point at 660 nm. Job's plot showed that the guest **63** was bound into **62** with a 1:1 stoichiometry. The related binding constant was estimated to be 3.6×10^4 M^{-1}.
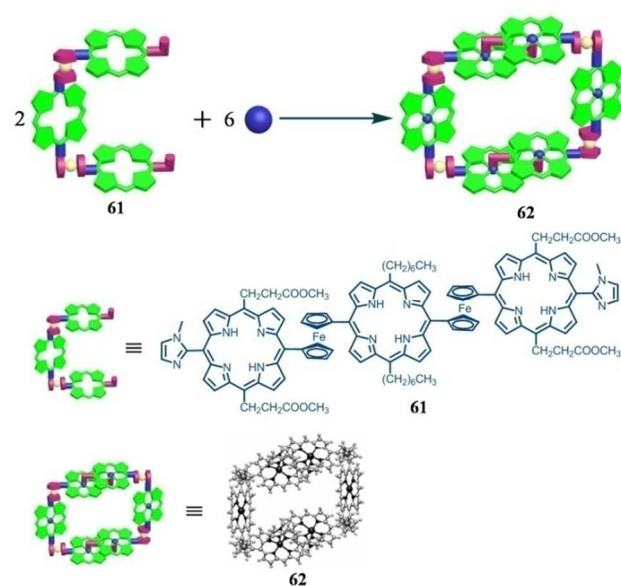

Fig. 23 Cartoon representation of the formation of tetrakisferrocenyl metallacycle **62** from ligand **61** and Zn(II) acetate; the crystal structure of **62**.
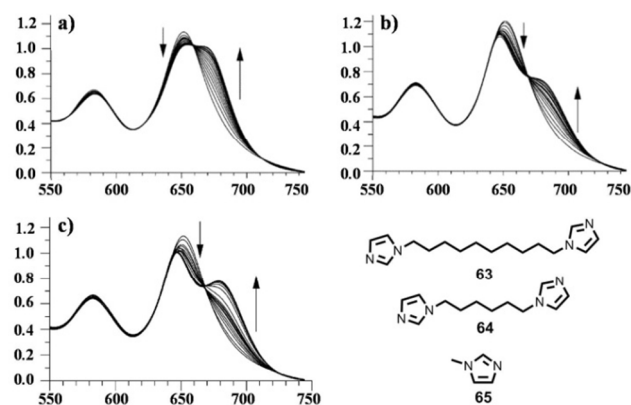

Fig. 24 UV−vis spectral change in **62** in chloroform induced by addition of **63** (a), **64** (b), and **65** (c) at room temperature. Copyright 2005 American Chemical Society.

Moreover, as shown in Fig. 24, the addition of bidentate ligands 1,3-di(1H-imidazol-1-yl)propane (**64**) or *N*-methylimidazole (**65**) exhibited the similar spectral change. The corresponding binding constants were evaluated to be 1.8×10^3 M^{-1} and 2.4×10^3 M^{-1}, respectively. The larger binding constant observed for guest **63** was a positive sign for cooperative binding inside the ring, while the relatively weak cooperativity of guests **64** or **65** with the metallacycle **62** was attributed to the sterically crowded interior of **62** and less flexible of guests **64** or *N*-methylimidazole **65** compared to that of **63**.

2.4 *Corner*-functionalized multiferrocenyl metallacycles

1, 1'-bis(diphenylphosphino)ferrocene (dppf), as a member of *syn*-1,1'-disubstituted ferrocene derivatives, has been extensively studied and used as a ligand to react with Pd(II) or Pt(II) to prepare ferrocene-chelated metallic acceptors. Since these acceptors provide sufficient rigidity at corners, they are suitable for the self-assembly of *corner*-functionalized multiferrocenyl metallacycles.
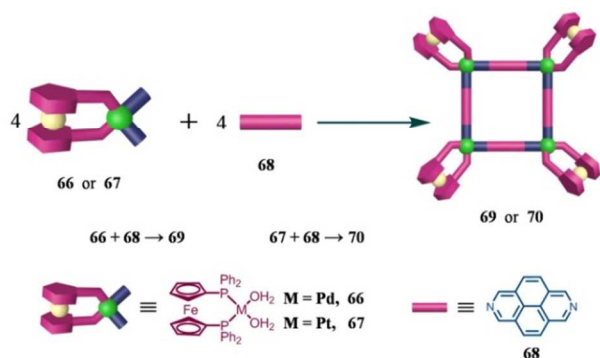
Fig. 25 Cartoon representation of the formation of multiferrocenyl squares **69** and **70** from acceptor **66** or **67** and linear donor **68**, respectively.
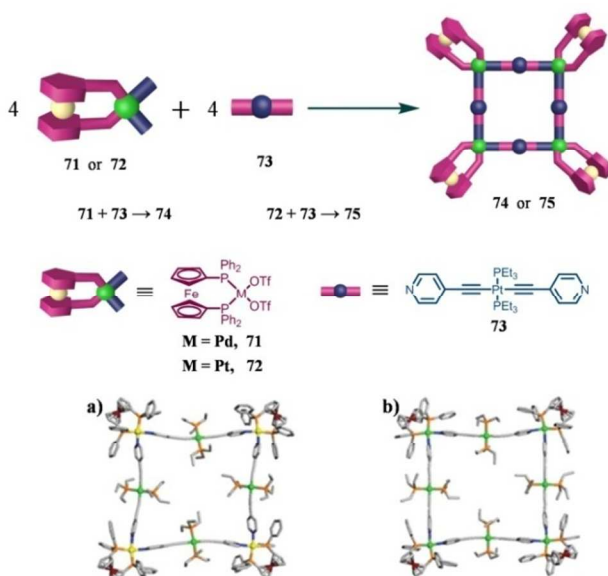

Fig. 26 Cartoon representation of the formation of squares **74** and **75** from acceptor **71** or **72** and linear donor **73**, respectively; the crystal structures of **74** (a) and **75** (b).

Stang *et al.* prepared two *corner*-functionalized multiferrocenyl squares **69** and **70** through the reaction of the complex 1,1'-bis(diphenylphosphino)ferrocene palladium(II) **66** or platinum(II) bis(triflates) **67** with 2,7-diazapyrene **68** in nitromethane at room temperature, respectively (Fig. 25).[33] Through the similar strategy, Stang and Chi *et al.* synthesized two squares **74** and **75** by stirring the mixture of 90° acceptors *cis*-(dppf)Pd(OTf)$_2$ **71** or *cis*-(dppf)Pt(OTf)$_2$ **72** with the linear donor *trans*-[(4-pyridylethynyl)$_2$Pt(PEt$_3$)$_2$] **73** in a 1:1 ratio at room temperature in a high yield (> 95%), respectively (Fig. 26).[34] The X-ray diffraction studies revealed that the complexes **74** and **75** featured different sized molecular cavities (Fig. 26). For instance, complex **74** had a square cavity of 5.5 × 5.8 Å with a bent geometry of ligand **73**, while complex **75** showed an elongated cavity with 20 × 4 Å with a straight geometry of ligand **73**.

Interestingly, unlike the formation of square **74** from symmetric donor **73**, Mukherjee *et al.* reported that stirring the mixture of *cis*-(dppf)Pd(OTf)$_2$ **71** with the nonsymmetric flexible donor sodium isonicotinate resulted in the formation of a triangle-square equilibrium.[35] Theoretically, the employment of the
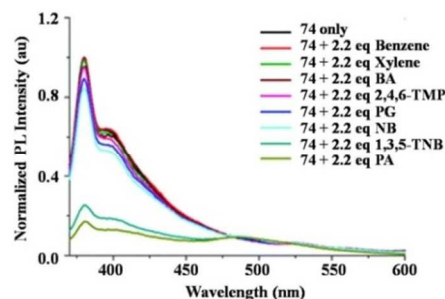

Fig. 27 Emission quenching of **74** upon the addition of the various guest molecules (1 × 10^{-4} M in THF). BA = benzoic acid, 2,4,6-TMP = 2,4,6-trimethylphenol, PG = phloroglucinol, 4-NB = 4-nitrobenzene, 1,3,5-TNB = 1,3,5-trinitrobenzene, PA = picric acid. Copyright 2011 Royal Society of Chemistry.

nonsymmetrical ambidentate ligand sodium isonicotinate was expected to form a complex mixture comprising several linkage isomeric squares and triangles as a result of different connectivity of the ambidentate linker. Surprisingly, only a mixture of symmetrical isomeric triangle and square was formed in this case. The equal electron density distribution around the Pd(II) centers was probably a reason for the formation of these two symmetrical linkage isomers. Moreover, Mukherjee *et al.* reported another example that the treatment of [M(dppf)(H$_2$O)$_2$](OTf)$_2$ (M = Pd, Pt) with 1.0 equiv of disodium fumarate in methanol medium showed an unusual hydrogenation of the ethylenic bond followed by the formation of metallochelates linking M through one of the carboxylates and the β-carbon with respect to COO$^-$.[36]

The presence of Pd-ethynyl or Pt-ethynyl functionality endowed the obtained squares **74** and **75** with the electron-rich and photoluminescent properties. Thus the detection of small molecules such as aromatic compounds by employing the squares **74** and **75** as hosts were investigated through the ways of absorption and emission studies. As shown in Fig. 27, no significant quenching was observed with the addition of electron-rich molecules like benzene, xylene, or 2,4,6-TMP, even at high concentration, to the solution of square **74**. A similar observation was obtained with the addition of polar aromatics like benzoic acid and phloroglucinol. However, when the electron-poor molecule like 1,3,5-TNB or picric acid was added into the solution of square **74**, an obvious emission quenching was observed. This result indicated that the increased electron-withdrawing nature of nitro-aromatics may induce an enhanced π–π interaction of nitro-aromatics with the π-electron rich molecular square **74**. Based on the emission quenching titrations with picric acid, the quenching constants (Ksv) were estimated to be *ca.* 6.72 × 10^5 M^{-1} for **74** and 7.00 × 10^5 M^{-1} for **75**, which indicated that **74** and **75** exhibited the high sensitivity to picric acid. The controlled experiments revealed that only a slight emission quenching in the presence of picric acid was found with ligand **73** and no quenching was observed in the case of **71**. This result confirmed the involvement of the donor centre during the quenching process and supported the enhanced response of these squares for the sensing of picric acid as well.

Azobenzene and its derivatives are known to undergo the efficient reversible photoisomerization reactions. Typically,
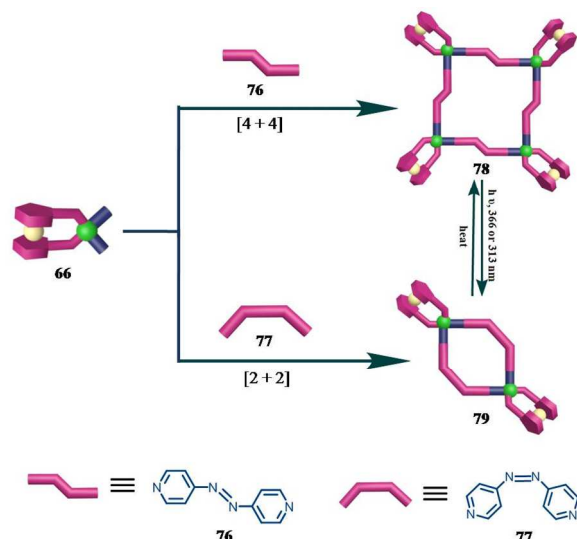
Fig. 28 Cartoon representation of the formation of squares **78** and **79** from 90° acceptor **66** and donor **76** or **77**, respectively.
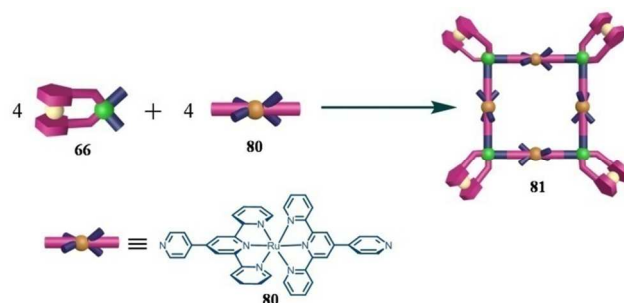
Fig. 29 Cartoon representation of the formation of tetrakisferrocenyl square **81** from 90° acceptor **66** and 180° donor **80**.

through irradiation with UV-light, the thermodynamically stable

5 *trans* isomer of azobenzene can be switched into the *cis* form, which can be converted back to the *trans* form by heating or exposure to the visible light. Thus, the incorporation of azobenzene moiety into the molecular structure to construct photoresponsive molecular systems has attracted great interest

10 because of their potential applications in the development of molecular or supramolecular devices. Lees *et al.* prepared two squares **78** and **79**, which were bridged by the photoisomerizable 4,4'-azopyridines (AZP) and cornered by ferrocenes, through self-assembly of 90° acceptor **66** with *trans*-AZP **76** or *cis*-AZP

15 **77** in CH$_2$Cl$_2$, respectively (Fig. 28).[37]

A photoinduced isomerization of **78** was observed as shown in Fig. 28. Upon irradiation of **78** at 313 nm in CH$_3$CN solution at 293 K, the absorption band at 282 nm slowly decreased and blue-shifted to 270 nm, while the band at 370 nm slowly increased and

20 reached a photostationary state after 20 h of irradiation. In this case, a ratio of tetramer (**78**) and dimer (**79**) was determined to be 2:3 evidenced by ^{31}P NMR data. Subsequently, the mixture of tetranuclear **78** and dinuclear **79** could be fully converted back to the tetranuclear species upon heating at 323 K for 1 h. This study

25 provided a successful construction of photoresponsive tetrakisferrocenyl square that could be photochemically converted to its corresponding bisferrocenyl square and thermally returned back to the tetrakisferrocenyl square.

The incorporation of luminescent transition-metal complexes,

30 Re(I)-, Ru(II)-, and Os(II)-based polypyridyl chromophores into the macrocyclic structures have been extensively studied in recent years.[38] These metallacycles exhibited not only the intriguing structures and interesting luminescent properties but also effective sensing for anions or certain aromatic compounds as a

35 consequence of Coulombic and/or hydrophobic interactions between the host and guest molecules. Lees *et al.* have realized the preparation of a Ru(II)-based tetrakisferrocenyl square **81** through reaction between (dppf)Pd(H$_2$O)$_2$(OTf)$_2$ **66** and (4'-(4-pyridyl)-2,2':6',2''-terpyridine)$_2$Ru(PF$_6$)$_2$ **80** in CH$_3$NO$_2$ solution

40 in high yield (95%) (Fig. 29).[38] Based on MM3 molecular modelling, the size of square **81** was determined to be 21.8 ×
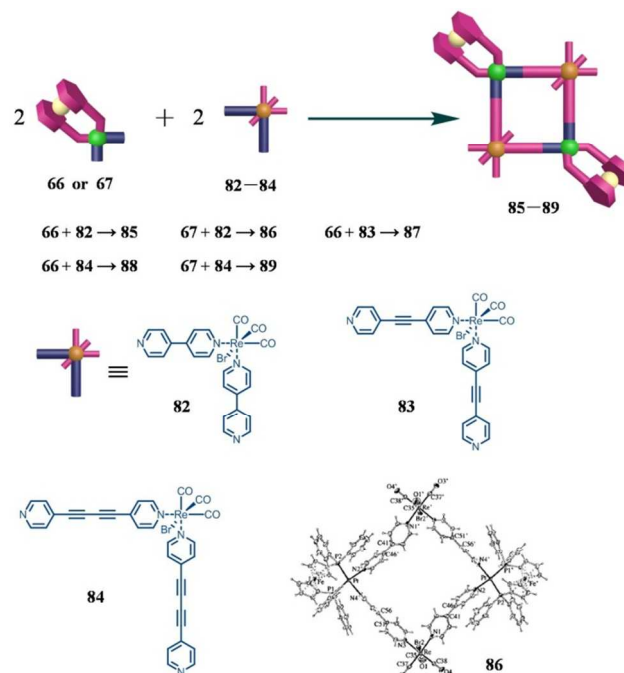

Fig. 30 Cartoon representation of the formation of squares **85–89**; the crystal structure of **86**.

21.8 Å, which was represented as one of the largest molecular squares. However, the effective internal cavity for square **81** was

50 much smaller than that measured from the edge due to the perpendicular arrangement of two terpyridine units around the center metals. Electronic absorption spectrum of square **81** displayed broad and intense visible absorptions in the region 400–600 nm and 250–350 nm, which were assigned to metal

55 (Ru)-to-ligand (4'-(4-pyridyl)-2,2':6',2''-terpyridine, pyterpy) charge transfer (MLCT) bands and pyterpy-based π-π* bands, respectively.

Recently, Lees *et al.* prepared another series of Re(I)-containing squares **85–89** by stirring the equivalent amount of

60 (dppf)M(H$_2$O)$_2$(OTf)$_2$ (M = Pd or Pt) and *fac*-BrRe(CO)$_3$(L)$_2$ (L = 4,4'-bpy, DPB, or DPA) in CH$_2$Cl$_2$ or CH$_3$NO$_2$ for 24 h in relatively high yields (87% for **85**, 79% for **86**, 42 % for **87**, 78% for **88**, and 81% for **89**) (Fig. 30).[39] The obtained crystal structure of **86** unambiguously confirmed the square geometry with a 11.28

65 × 11.38 Å cavity as defined by the distances between Re(I) and Pt(II). Cyclic voltammetric experiments of **85–89** revealed two oxidation potentials for all the square complexes. According to the oxidation potentials of the Re(I)-based corners and

(dppf)Pt(H$_2$O)$_2$(OTf)$_2$, two reversible oxidation processes were attributed to Fe$^{2+/3+}$ and Re$^{1+/2+}$, respectively.

The well-defined structures, positive charges, and luminescent properties of the squares **85**–**89** rendered them as the potentially effective hosts for anionic species. For instance, the addition of PF$_6^-$ or BF$_4^-$ induced the significant changes of luminescence intensities of squares **85**–**89**. As shown in Fig. 31, the luminescence intensity first decreased when a small amount of BF$_4^-$ was added to square **85** in acetone solution. However, the luminescence intensity then started to increase and finally reached a plateau when the amount of the added BF$_4^-$ apparently rised over a critical concentration. Similar results were also observed for the other luminescent squares **86**–**89** when the PF$_6^-$ was employed as guest. The simple anion exchange process was ruled out by such unusual change of the emission intensity upon the addition of PF$_6^-$ and BF$_4^-$. No significant change of luminescence intensity was observed with the addition of ClO$_4^-$, OAc$^-$, or OTf$^-$. The selective sensing of PF$_6^-$ and BF$_4^-$ might be attributed to the anion encapsulation inside the square cavity and the electrostatic induced ion-pair interaction between the square and anion.

In recent years, the design of multicationic supramolecular architectures that can noncovalently bind the major groove of DNA and cause the remarkable intramolecular DNA coiling has been of great interest owing to their applications in probing biological systems and developing therapeutic drugs.[40] Recently, Chi *et al.* constructed two tetracationic heterobimetallacycles **91** and **92** through reaction of the acceptors *cis*-Pd[(dppf)(OTf)$_2$] (**71**)
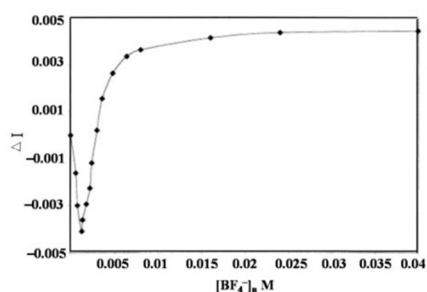

Fig. 31 Binding isotherm depicting change of emission of square **85** upon addition of ^{n}Bu$_4$BF$_4$ in acetone solution. Copyright 2002 American Chemical Society.
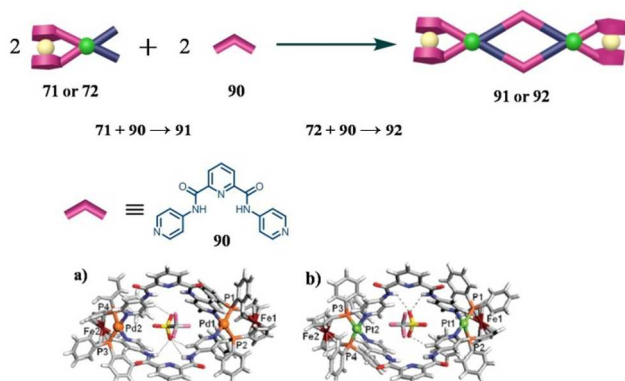

Fig. 32 Cartoon representation of the formation of metallacycles **91** and **92** from acceptor **71** or **72** and donor **90**, respectively; the crystal structures of **91** (a) and **92** (b).

or *cis*-Pt[(dppf)(OTf)$_2$] (**72**) with the donor **90** at room temperature in a [2 + 2] manner, respectively (Fig. 32).[40] The structures of metallacycles **91** and **92** were fully characterized by X-ray diffraction study. As shown in Fig. 32, the ferrocenyl moieties occupied the outlying sites on the partially distorted square planar Pd(II) or Pt(II) center. More importantly, the crystal structures of both complexes showed that an anionic molecule was captured in the cavity through hydrogen-bonding interactions.

The interactions of **91** and **92** with supercoiled DNA were examined through photophysical and gel electrophoresis methods (Fig. 33). Upon addition of DNA, the absorption peaks at 266 nm for **91** or 270 nm for **92**, corresponding to the intraligand π−π* transition, showed the significant hypochromic shifts. These results suggested that the complexes **91** and **92** were bound to DNA through intercalation. The binding constants (K_b) of **91** or **92** with DNA were calculated to be 2.58×10^5 M^{-1} and 1.23×10^5 M^{-1}, respectively, which revealed that **91** bound more efficiently to DNA than that of **92**. The binding of the complexes **91** or **92** to DNA were further investigated by a fluorescence spectroscopic method using the emission intensity of ethidium bromide (EtBr) as a probe. The combining of the complex to DNA could be displaced by EtBr, thereby decreasing its emission intensity (quenching). The ratio of the slope to the intercept obtained by plotting I_0/I vs [Q] yielded values of K_q corresponding to 3.86×10^3 M^{-1} for **91** and 2.14×10^3 M^{-1} for **92**, which indicated that the **91** featured a higher quenching efficiency than that of **92**.

The DNA relaxation activity of the complexes **91** and **92** were investigated by gel electrophoresis studies. The results revealed that the metallacycle **92** exhibited the higher efficiency than **91** when unwinding DNA, indicating that the complex **92** featured a high intercalation capacity. Moreover, the controlled experiments established that neither the metal acceptors **71** and **72** nor the donor **90** had such relaxation activity. Thus, the interaction of metallacyclic complexes with DNA was responsible for the observed relaxation behaviour.
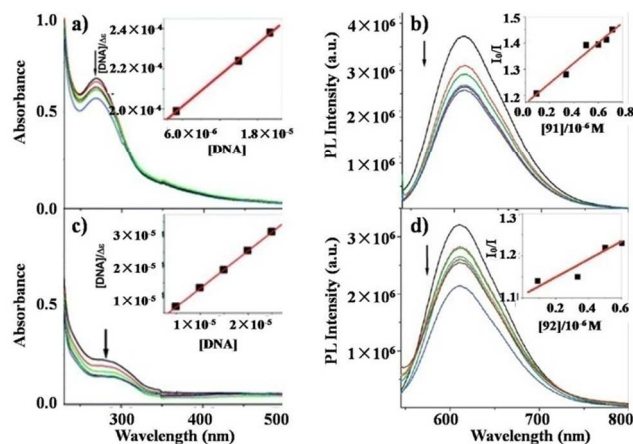

Fig. 33 (left) UV/vis absorption spectra of **91** (a) and **92** (c) upon incremental addition of DNA. Insets give binding constant plots for the supercoiled DNA-HBMCs. (right) Emission spectra of **91** (b) and **92** (d) upon gradual addition of DNA (EB bound). Insets give Stern–Volmer plots for the supercoiled DNA-HBMCs. Copyright 2011 American Chemical Society.

3. Multiferrocenyl metallacages

Compared with the self-assembled 2-D metallacycles, in general, the 3-D metallacages with different shapes and sizes display the advantages when applying in the fields of selective guest encapsulation and recognition, cavity induced catalysis, sensing, and even gas storage.[8] Over the past two decades, there has been a tremendous increase in the construction of well-defined organometallic polyhedra including multiferrocenyl metallacages.[9]

3.1 *Exo*-functionalized multiferrocenyl metallacages

Generally, supramolecular organometallic cuboctahedra can be obtained through the combination of twelve 120° molecular subunits with eight complementary planar tritopic subunits. Stang and White *et al.* successfully realized the construction of cuboctahedral complex **94** decorated with twelve pendant ferrocenes at the vertexes by stirring a mixture of the ferrocenyl 120° di-Pt(II) acceptor **21** and the linear tritopic donor **93** in a 3:2 ratio (Fig. 34).[41]

Multinuclear NMR {^{1}H and ^{31}P} spectroscopy, elemental analysis, and ESI-MS results provided the strong evidences for the formation of such multi-ferrocenyl cuboctahedron **94**. For example, the ^{31}P {^{1}H} NMR spectrum of **94** displayed a sharp singlet (~16.9 ppm) shifted upfield from that of the starting platinum acceptor **21** by ~6.0 ppm. This change, as well as the decrease in coupling of the flanking ^{195}Pt satellites ($\Delta J = -63.2$ Hz), was consistent with back-donation from the platinum atoms. Additionally, the ESI-MS spectrum showed peaks at m/z 3383.8, 2879.0, and 2501.0 corresponding to $[M - 6OTf]^{6+}$, $[M - 7OTf]^{7+}$,
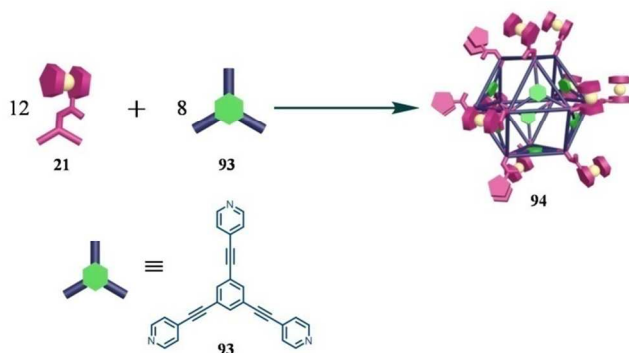
and $[M - 8OTf]^{8+}$, respectively. Molecular force field simulation revealed that **94** featured a well-defined cuboctahedron with an approximate diameter of 6.7 nm and an internal cavity size of ~5.0 nm, and the distance between adjacent ferrocene units was 2.9 nm.

The electrochemical property investigation of multiferrocenyl cuboctahedron **94** discolsed a single redox wave, suggesting that there was no interaction among the multiple redox centers at the periphery (Fig. 35). Electrochemical reversibility revealed fast electron transfer among the flexible peripheral redox sites, which could be explained by fast rotation or as the result of electrons hopping through space. This example provided a general strategy for the synthesis of stable, multifunctional cuboctahedral complexes, in which coordination-driven self-assembly allowed for precise control over the position of ferrocenyl functionality. Considering the fact that the multiferrocenes in complex **94** are active at one single potential over various scan rates, it may find potential applications as multielectron catalysts or sensors.

Recently, Crowley *et al.* synthesized a 0° donor building block **95** attached with a ferrocenyl group on the periphery through the click methodology (Fig. 36).[42] Stirring the mixture of **95** and $[Pd(CH_3CN)_4](BF_4)_2$ in either d_6-DMSO or CD_3CN in a 2:1 stoichiometric ratio, the metallacage **96** decorated with four pendant ferrocenes at the vertexes was prepared in nearly quantitative yield through coordination-driven self-assembly. The structure of cage **96** was unambiguously confirmed by X-ray crystallography (Fig. 36a), which revealed the palladium(II) ions coordinated to the terminal pyridine rings rather than the *endo*-pyridine or *exo*-triazole moieties.

The investigation of host-guest chemistry indicated that cage **96** exhibited good encapsulation efficiency for cisplatin. The host–guest interaction of **96** and cisplatin was proven by using X-ray crystallography (Fig. 36b), which displayed a co-crystal of both the empty cage complex **96** and the intended 1 : 2 host–guest species **96**⊃(cisplatin)$_2$, with the crystal lattice containing alternating chains of these two species. Moreover, judging from the distance between opposing endohedral pyridyl nitrogen atoms

Fig. 34 Cartoon representation of the formation of cuboctahedral complex **94** from 120° acceptor **21** and the linear donor **93**.
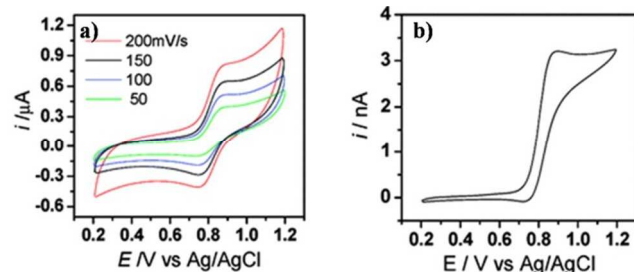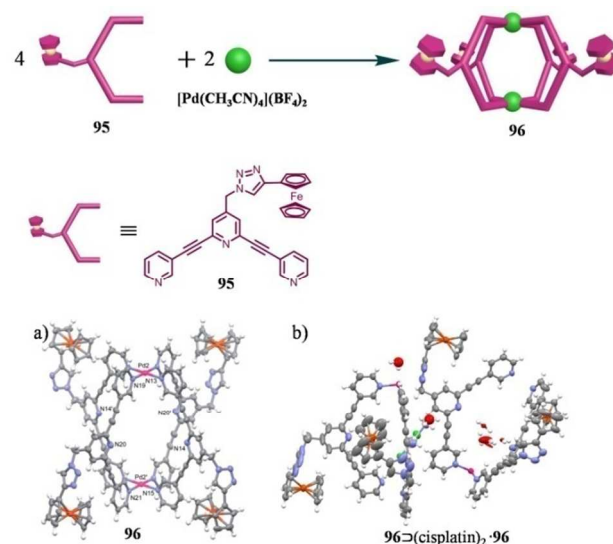

Fig. 35 (a) Cyclic voltametry of **94** at different scan rates (50−200 mV/s) at a 1 mm^2 Pt electrode. (b) Steady-state current response of **94** at 20 mV/s at a microsized (26 μm diameter) Pt disk electrode. Solution: 0.2 mM **94** in acetone containing 0.1 M n-Bu$_4$NPF$_6$. Copyright 2009 American Chemical Society.

Fig. 36 Cartoon representation of the formation of cage **96** from 0° donor **95** and $[Pd(CH_3CN)_4](BF_4)_2$; the crystal structures of **96** (a) and ellipsoid plot of the asymmetric unit of **96**⊃(cisplatin)$_2$ ·**96** (b).
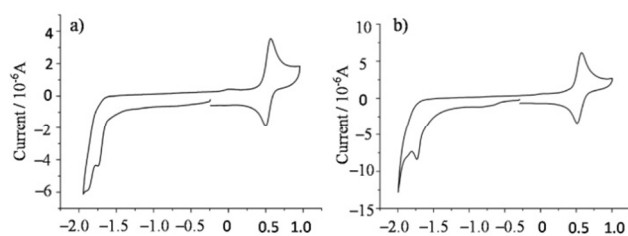
Fig. 37 Cyclic voltammogram of **95** (a) and **96** (b). Copyright 2014 Royal Society of Chemistry.

(10.5–10.9 Å) and the distance between palladium(II) ions (approximately 11.6 Å for both), the empty cage **96** and the host–guest assembly displayed very similar dimensions.

The redox properties of both ligand **95** and cage **96** in DMF solution were examined with cyclic voltammetry as well. As shown in Fig. 37, both of them displayed irreversible reductions at negative potentials (*ca.* −1.7 and −1.9 V), which were presumed to be associated with the 2,6-bis(ethynyl)pyridine ligand framework. Moreover, the ferrocenyl-substituted ligand **95** and cage **96** displayed the expected reversible oxidation of the ferrocenyl moiety at ~0.5 V. These findings demonstrated that the complexation of the ligands with palladium(II) ions to generate the cage **96** did not affect the potential or reversibility of any redox process and no electronic communication happened between the four redox active units of the cages.

Multicomponent self-assembly is a widespread phenomenon in biological systems. However, the self-assembly of three or more components in supramolecular chemistry is sometimes plagued by the formation of entropically favored, disordered oligomers, or dynamic mixtures. Therefore, the development of efficient method to the self-assembly of discrete supramolecular structures with well-controllable sizes and shapes from more than two distinct tectons has attracted much attention. Recent research has revealed that three-component systems composed of square planar Pt(II) center, pyridine, and anionic carboxylate donors could self-assemble into multicomponent supramolecular rectangles or prisms with high efficiency.[43] According to this strategy, Stang *et al.* constructed a tetragonal prism **100** decorated with four ferrocenes through the combination of tetra-(4-pyridylphenyl)ethylene **97**, *cis*-(PEt$_3$)$_2$Pt(OTf)$_2$ **98**, and ferrocenyl-functionalized ditopic carboxylate ligand **99** in a ratio of 1:4:2 in acetone/nitromethane (v/v , 2/1) (Fig. 38).[44]

It is worthy to be noted that the ^{31}P {^{1}H} NMR spectrum of **100** displayed four doublets with approximately equal intensities
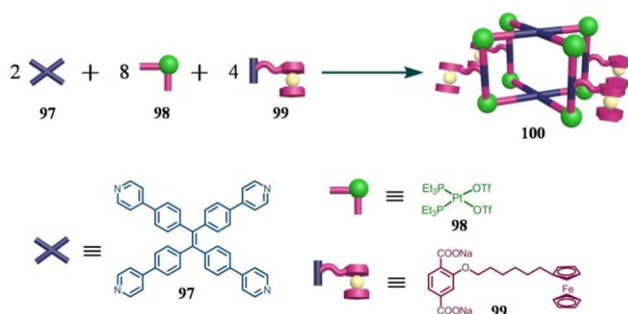
at δ = 6.80, 6.10, 1.28, and 1.21 ppm, respectively, corresponding to two sets of coupled phosphorus atoms. The presence of four doublets indicated the distinct phosphorus environments, which was indicative of heteroligated coordination of pyridine and asymmetric carboxylate to each platinum center. PGSE NMR measurement further indicated that **100** was a well-defined tetragonal prism with a diameter of 2.43 ± 0.19 nm.

The properties of the above mentioned assemblies, which are usually predetermined by the molecular building blocks used, are generally inherent to the final structure, thus being fixed upon self-assembly. Recently, owing to the advantage of tailoring the properties of supramolecular assemblies after initial self-assembly, post-self-assembly modification strategy has been successfully employed to build functional architectures.[45] Post-self-assembly modification strategy allows for the further tuning of a supramolecular species to achieve desired structures with high complexity and additional functionality after initial self-assembly, thus resulting in the modifiable supramolecular systems.

Post-self-assembly covalent modification usually employs the certain organic reactions to efficiently introduce new moieties onto a supramolecular structure bearing functional sites. It is well-known that the maleimide group allows for the efficient Diels-Alder reaction with other functionalized anthracene derivatives to incorporate new functionality under mild condition. Recently, Stang and White *et al.* reported the preparation of hexagonal prism **103** decorated with maleimide groups through self-assembly of hexakis[4-(4-pyridyl)phenyl]benzene **101**, 90° Pt(II) acceptor **98**, and 5-maleimideisophthalate **102** (Fig. 39).[45] Subsequently, the covalent post-synthetic modification of hexagonal prism **103** yielded multiferroces-functionalized hexagonal prism **105** by treating **103** with (9-methylene anthracenyl)-1-ferrocenoate **104** in a ratio of 1:5 in nitromethane-d_3 solutions *via* Diels-Alder reaction.

The hexagonal prisms **103** and **105** were characterized with multinuclear NMR, ESI-MS, molecular-force field simulations, and PGSE NMR experiments. These results firmly supported the complete conversion of hexagonal prism **103** into the post-
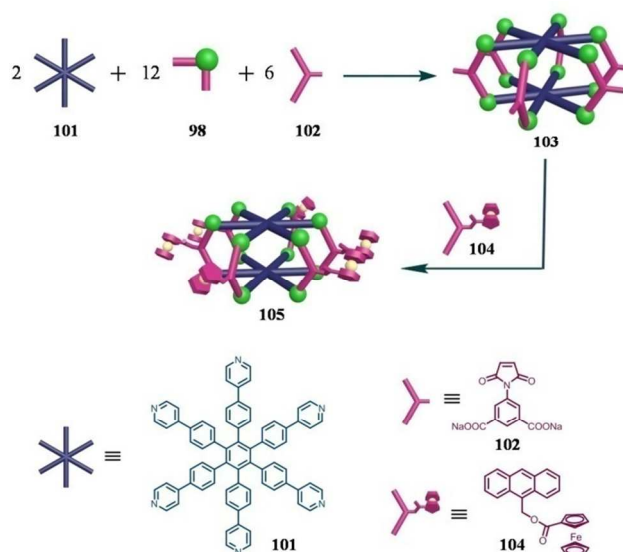

Fig. 38 Cartoon representation of the formation of tetragonal prism **100** from **97**, **98**, and **99**.

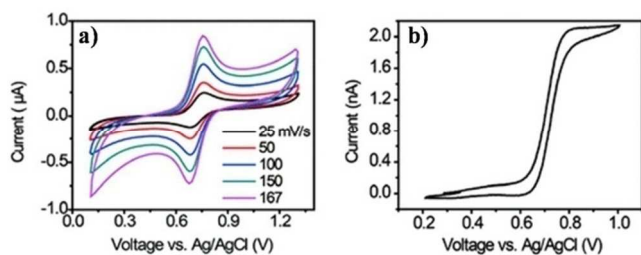**Fig. 39** Cartoon representation of the formation of hexagonal prisms **103** and **105**.

Fig. 40 (a) Cyclic voltametry of **105** at different scan rates (25–167 mV/s) at a ~0.5 mm^2 Pt electrode; (b) Steady-state current response of compound **105** at 30 mV/s at a ~25 μm diameter Pt disk electrode. Solution: 0.2 mM **105** in acetonitrile containing 0.1 M n-BuN$_4$PF$_6$. Copyright 2011 American Chemical Society.

synthetically modified species **105** maintaining the integrity of the prismatic core. For instance, similar to that of **100**, the ^{31}P {^{1}H} NMR spectra of **103** and **105** displayed two doublets with approximately equal intensities, which corresponded to the two distinct phosphorus environments of the prisms. More importantly, in the ^{1}H NMR spectrum of **105**, the signals corresponding to the protons of isophthalate displayed downfield shifts compared to those of **103**. Furthermore, new peaks at δ = 5.61, 4.95, 4.85, 4.79, 4.53, and 4.37 ppm, corresponding to the cycloaddition of (9-methylene anthracenyl)-1-ferrocenoate for **105**, were observed. Cyclic voltammetry (CV) studies of **105** displayed a single redox wave, which suggested the existence of ferrocene moieties (Fig. 40). No redox event was observed in the controlled CV investigation of **103**, further verifying that the ferrocenyl groups were incorporated into **105**.

Therefore, post-self-assembly modification strategy provides an alternative approach to construct functionalized metallosupramolecules. In particular, it is very helpful for the construction of species that are not accessible *via* conventional coordination-driven self-assembly. This post-synthetic approach is a promising way to unlock the new applications and behaviours of the supramolecular assemblies.

3.2 *Edge*-functionalized multiferrocenyl metallacages

Recently, Raymond *et al.* prepared a novel ferrocene-based biscatecholamide ligand **106**, which was found to be coordinated with metal Ge^{4+} in DMF-d_7 to afford the mixture complexes of [Ge$_2$L$_3$]$^{4-}$ helix **107** and [Ge$_4$L$_6$]$^{8-}$ tetrahedron **108** (Fig. 41).[46] In general, the self-assembly of similar ligand, such as the benzene-based biscatecholamide ligand **109** or naphthalene-based biscatecholamide ligand **110**, with Ge^{4+} yielded a discrete triplestranded metallohelicate or tetrahedral assembly, respectively. Herein the formation of mixture assemblies of ligand **106** with Ge^{4+} was ascribed to the relative flexibility of ferrocene linker. Surprisingly, the addition of CD$_3$OD into the DMF-d_7 solution of the obtained mixture of **107** and **108** resulted in the quantitative formation of a single new complex **111**, which was further characterized with NMR spectroscopy, mass spectrometry, and X-ray crystallographic analysis (Fig. 41).

The X-ray diffraction experiment revealed that the complex **111** was correctly formulated as [Ge$_2$L$_2$(μ-OMe)$_2$]$^{2-}$, where each Ge atom was chelated by one ferrocenyl ligand and the methoxide groups bridged the two octahedrally coordinated Ge atoms. Interestingly, with the addition of EtOH or ^{i}PrOH into the DMF-d_7 solution of the obtained mixture of **107** and **108**,
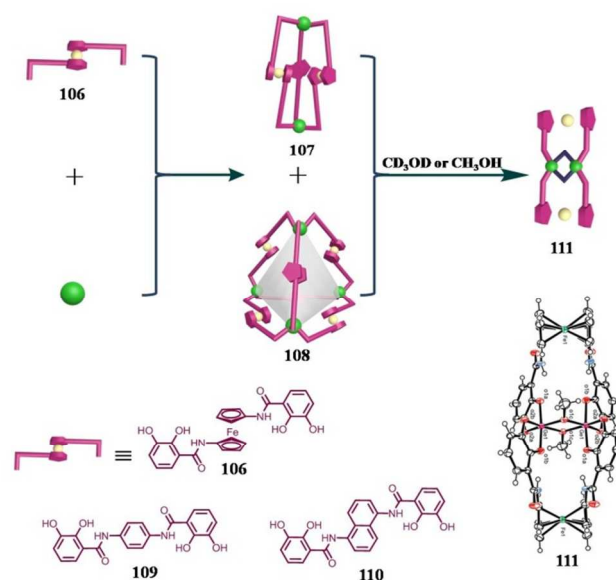

Fig. 41 Cartoon representation of the formation of complex **111**; the crystal structure of **111**.

respectively, neither the analogous [Ge$_2$L$_2$(OEt)$_2$]$^{2-}$ nor [Ge$_2$L$_2$(O^{i}Pr)$_2$]$^{2-}$ complexes were formed. The investigations of the molecular mechanics-minimized models of the [Ge$_2$L$_2$(OEt)$_2$]$^{2-}$ and [Ge$_2$L$_2$(O^{i}Pr)$_2$]$^{2-}$ complexes indicated that the OEt and O^{i}Pr fragments were too large to serve as bridging ligands.

3.3 *Corner*-functionalized multiferrocenyl metallacages

Similar to the construction of *corner*-functionalized multiferrocenyl metallacycles, the self-assembly of *cis*-Pd[(dppf)(OTf)$_2$] or *cis*-Pt[(dppf)(OTf)$_2$] with tritopic ligand could lead to the generation of *corner*-functionalized multiferrocenyl metallacage. It is well-known that the highly symmetric octahedral M$_6$L$_4$ structure can be synthesized by the self-assembly of six 90° ditopic metal units (M) with four 120° planar tritopic ligand units (L).[8] Recently, Yang *et al.* reported the preparation of *corner*-functionalized hexakisferrocenyl metallacage **113** through the facile self-assembly of 90° *cis*-(dppf)Pd(OTf)$_2$ **71** and 120° tritopic 2,4,6-tri(4-pyridyl)-1,3,5-triazine ligand **112** in a ratio of 3:2 in acetone solution (Fig. 42).[47]
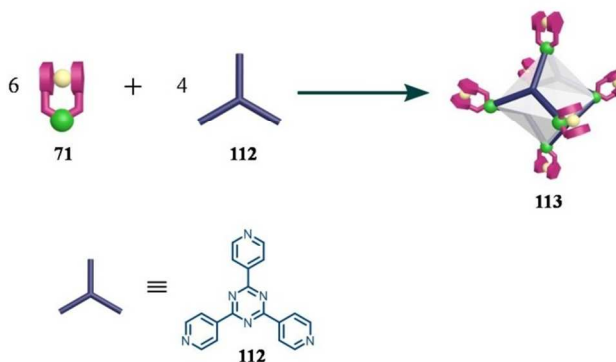

Fig. 42 Cartoon representation of the formation of hexakisferrocenyl metallacage **113** from 90° acceptor **71** and 120° donor **112**.
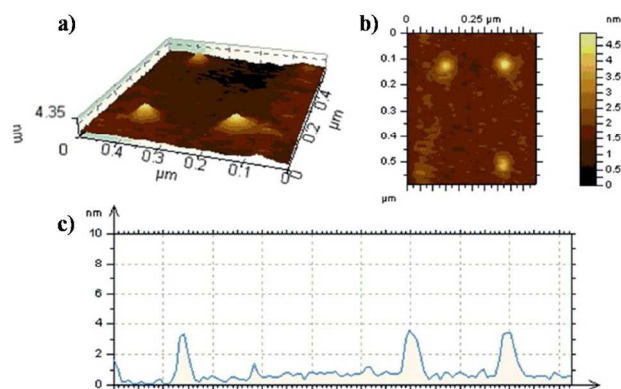
Fig. 43 AFM images of metallacage **113** on mica: a) 3D image, b) 2D image and c) height profile. Copyright 2013 Wiley-VCH.
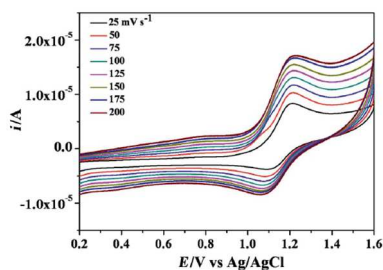

Fig. 44 Cyclic voltammetry of **113** at different scan rates (25–200 mVs⁻¹) at a 3 mm diameter glassy carbon working electrode in 0.3 mm acetone solution containing 0.1 M *n*-Bu₄NPF₆, vs. Ag/AgCl. Copyright 2013 Wiley-VCH.

The AFM study of **113** clearly indicated that the diameter of **113** was approximately 3–4 nm (Fig. 43). Furthermore, the calculated diameter of **113** was in good agreement with those obtained from the DOSY deduced results and AFM observations. Cyclic voltammograms of **113** displayed a considerably broad voltammetric peak, which was probably attributed to the simultaneous statistical nature of the multielectron transfer processes (Fig. 44). Moreover, owing to the presence of triazine groups, the metallacage **113** was extremely electron-deficient, which provided a nanoscopic hollow environment that may potentially sense electron-rich guests.

Similar to the preparation of **113**, a series of admantanoid-shaped metallacages **115–118** were constructed by Lees *et al.* by stirring the mixture of 90° acceptors *cis*-(dppf)Pd(OTf)₂ **71** or *cis*-(dppf)Pt(OTf)₂ **72** with tridentate pyridyl donors **93** or **114** in a molar ratio of 3:2 in CH₂Cl₂, respectively (Fig. 45).[48]

Tetrathiafulvalene (TTF) and its derivatives, as electron donors in organic charge-transfer materials, have been extensively investigated in the field of organic conductors, superconductors, and supramolecular switchable systems. Recently, Goeb and Sallé et al. synthesized a TTF-containing donor **119** from pristine TTF through a Palladium-catalyzed C–H cross-coupling reaction with 4-iodopyrine (Fig. 46).[49] The XRD analysis of ligand **119** revealed that the TTF skeleton and the four nitrogen atoms were coplanar and set in a rectangle defined by a length of 13.1 Å and a width of 6.7 Å. The coordination-driven self-assembly of **119** with cis-Pd(dppf)(OTf)₂ **71** or cis-Pt(dppf)(OTf)₂ **72** in nitromethane at 50 °C was investigated, respectively (Fig. 46). Theoretically, depending on the orientation
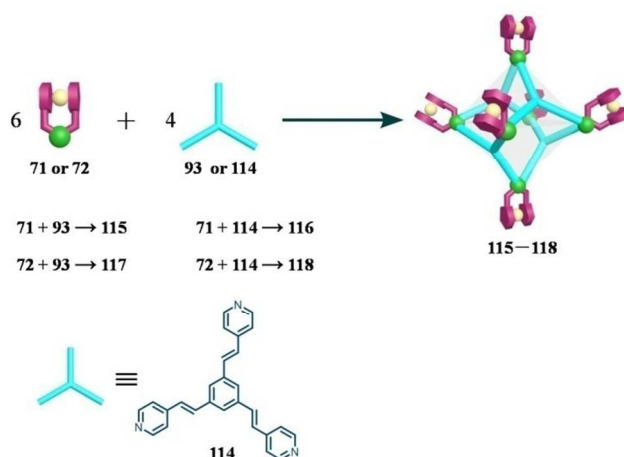

Fig. 45 Cartoon representation of the formation of admantanoid-shaped metallacages **115–118**.
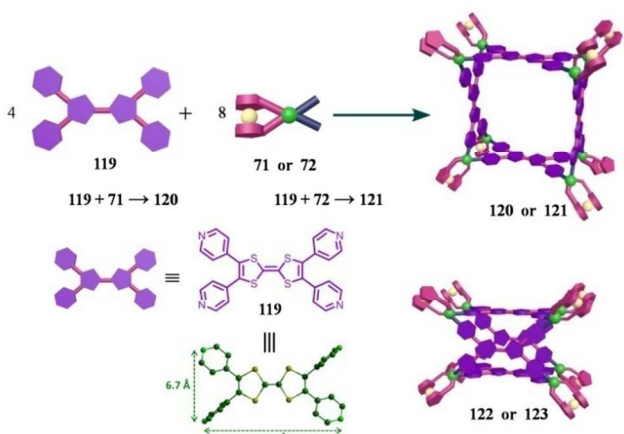

Fig. 46 Cartoon representation of the formation of metallacages **120** and **121** from donor **119** and acceptor **71** or **72**; the crystal structure of **119**.
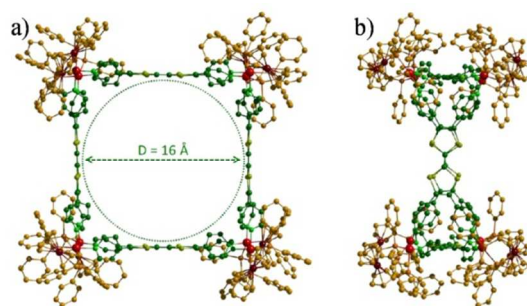

Fig. 47 Molecular force field (MM+) model of square **121**; (a) front view and (b) side view. Copyright 2014 MDPI.

of the ligands inside the structure, two types of geometry were conceivable for the M₄L₈ assemblies (i.e., the rectangular ligands were connected to the metal centers through their short (**120** or **121**) or long side (**122** or **123**)). However, molecular force field (MM+) studies revealed that the symmetric stationary point for the assembly **122** or **123** could not be yielded due to a high structural strain while the highly symmetric assembly **120** or **121** could be reached (Fig. 47). Furthermore, the distance between two facing TTF plans was found to be 16 Å.

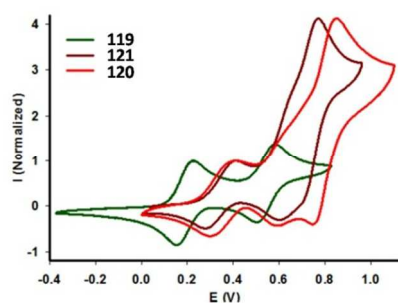Redox properties of ligand **119**, complexes **120** and **121** were

Fig. 48 Cyclic voltammogram of ligand **119** and squares **120** and **121**. Copyright 2014 MDPI.

studied by cyclic voltammetry (Fig. 48). As usually observed
5 with TTF derivatives, two reversible oxidation waves, which assigning to the successive generation of the cation-radical and dication states, were observed for ligand **119**. However, in the case of the self-assembled metallacages **120** and **121**, three reversible redox processes were observed. The first two were
10 assigned to the TTF side walls and the third one to the corner ferrocene units. Interestingly, the latter could be used as an internal reference to address the number of electrons exchanged along the redox processes.

The construction of porphyrin-based discrete assemblies has
15 been of great interest because of the important applications of porphyrin in biological systems for oxygen transport, energy conversion, and electron transfer. Recently, Mukherjee *et al.* investigated the self-assembly of tetratopic donor linker 5,10,15,20-tetrakis(4-pyridyl)porphyrin **124** with two equivalents
20 of 90° acceptor *cis*-(dppf)Pt(OTf)$_2$ **72** (Fig. 49).[50] From the combination of ligands **124** and **72**, the hexagonal open box **125** containing six porphyrin walls was obtained. The crystal structure of **125** clearly demonstrated that the six porphyrin-based units were hinged by twelve ferrocenyl *cis*-{(dppf)Pt}$^{2+}$ building
25 blocks to form Pt$_6$ hexameric rings on the top and bottom of the box. The box structure of **125** was rigid and the inner cavity was extraordinarily large with a dimension of $27 \times 27 \times 19$Å. Twelve ferrocenes were located at each vertex of hexagonal box **125**.

Hexagonal box **125** possessed six porphyrin pockets, which
30 might display the high encapsulating efficiency toward Zn^{2+}.
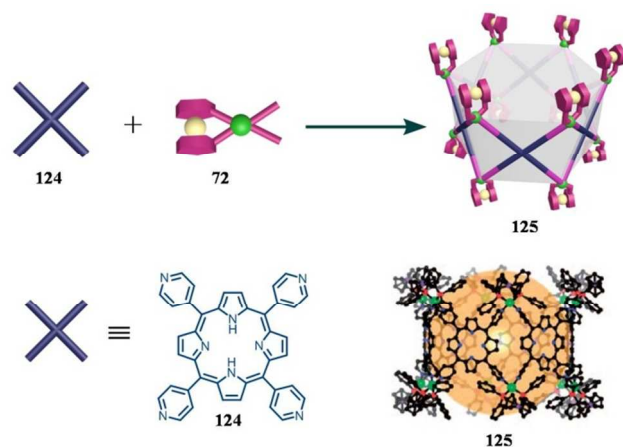

Fig. 49 Cartoon representation of the formation of hexagonal box **125** from donor **124** and 90° acceptor **72**; the crystal structure of **125**.
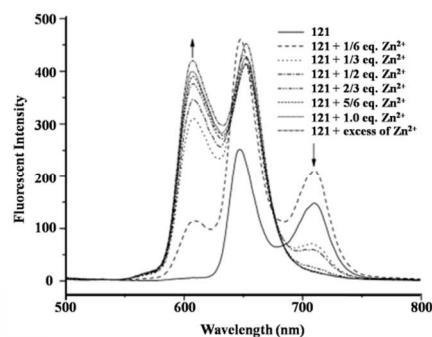

35 **Fig. 50** Emission fluorescence spectra of a methanolic solution of **125** (2×10^{-6} M) upon addition of increasing amounts of Zn^{2+}. Copyright 2008 Wiley-VCH.

Therefore, the titration of **125** with Zn^{2+} was carried out as well. As shown in Fig. 50, upon addition of a 1/6 equivalent of Zn^{2+} to
40 a methanolic solution of **125**, the enhancement of the emission bands at 646 and 709 nm along with the development of new band at 609 nm was observed. While increasing the amount of Zn^{2+} induced an obvious quenching of emission at 709 nm. Such spectral changes were caused by the binding of the Zn^{2+} in the
45 porphyrin N$_4$ pocket. The results indicated that **125** displayed high sensitivity to Zn^{2+}. Thus, **125** could be used as an optical sensor for Zn^{2+} and would have applications in environmental and biomedical fields.

Conclusions

50 This article systematically summarized the recent progress on the construction of multiferrocenyl metallacycles and metallacages *via* coordination-driven self-assembly. The above-mentioned examples demonstrate that coordination-driven self-assembly serves as a simple yet highly efficient approach to the
55 construction of multiferrocenyl organometallic architectures. Since ferrocene features a specific sandwich-type organometallic scaffold with relative rigidity as well as rich derivatization sites, ferrocenes could be incorporated into the outside, inside or as the edge and the corner of discrete multiferrocenyl metallacycles and
60 metallacages. Moreover, through the combination of complementary precursors substituted with different functional moieties, the construction of heterofunctional multiferrocenyl metallacycles was successfully realized *via* coordination-driven self-assembly strategy. In addition, the structure-related
65 electrochemical properties and applications of these multiferrocenyl metallosupramolecular structures, such as sensing metal ions, anions, neutral small molecules, and the interaction with DNA, were discussed in this article.

It is noteworthy that major efforts in this area have been
70 focused on the construction and characterization of structurally different multiferrocenyl metallacycles and metallacages during the past two decades. However, relatively less attention has been paid to the properties and applications of these novel assemblies. It is time to shift the research focus toward the new applications
75 of the multiferrocenyl architectures. In our opinion, three important aspects of the application should be considered in the future development of these supramolecular assemblies. Firstly, because of the wide applications of the ferrocene derivatives in catalysis, these multiferrocenyl metallacycles and metallacages

possessing well-defined cavities can be employed as ligands or molecular flasks in catalysis. It is worth noting that the presence of the cavities may be beneficial to improve the catalytic activities and selectivity. Secondly, the considerable change of the binding ability between ferrocene derivatives and β-cyclodextrin or pillar[n]arene before and after the oxidation of ferrocene moiety endows these multiferrocenyl metallacycles and metallacages great opportunities in the construction of stimuli-responsive "smart" materials through hierarchical self-assembly. Thirdly, the fact that some ferrocene derivatives show good antimalarial and anticancer activities offers the possible application of the multiferrocenyl metallacycles and metallacages in biological systems. Of course, water soluble metallacycles and metallacages should be constructed.

Compared to *non*-ferrocene metallacycles or metallacages, the multiferrocenyl metallacycles and metallacages may have many advantages in terms of their above mentioned applications. For example, the ferrocenyl moiety can be employed as the catalytic site to enhance the catalytic efficiency and selectivity of the resultant multiferrocenyl organometallic architectures. In addition, taking advantages of their redox properties and the host-guest capabilities with *β*-cyclodextrin or pillar[n]arene, ferrocene moieties can be used as the stimulus-response moiety to construct stimuli-responsive "smart" materials. Considering the aesthetically pleasing structures and wide applications of multiferrocenyl metallacycles and metallacages, it is believed that these multiferrocenyl metallosupramolecular architectures will receive more and more attention and play important role within supramolecular chemistry and materials sciences during the next decade.

Acknowledgements

Notes and references

Shanghai Key Laboratory of Green Chemistry and Chemical Processes, Department of Chemistry, East China Normal University, 3663 N. Zhongshan Road, Shanghai, 200062, People's Republic of China. Fax: (+86) 21-62235137; Tel: (+86) 21-62235137; E-mail: hbyang@chem.ecnu.edu.cn

1   H. Werner, *Angew. Chem. Int. Ed.*, 2012, **51**, 6052.
2   T. J. Kealy and P. L. Pauson, *Nature*, 1951, **168**, 1039.
3   D. R. van Staveren and N. Metzler-Nolte, *Chem. Rev.*, 2004, **104**, 5931.
4   T. J. Colacot, *Chem. Rev.*, 2003, **103**, 3101.
5   B. Fabre, *Acc. Chem. Res.*, 2010, **43**, 1509.
6   A. K. Diallo, C. Absalon, J. Ruiz and D. Astruc, *J. Am. Chem. Soc.*, 2011, **133**, 629.
7   D. Astruc, C. Ornelas and J. Ruiz, *Acc. Chem. Res.*, 2008, **41**, 841.
8   R. Chakrabarty, P. S. Mukherjee and P. J. Stang, *Chem. Rev.*, 2011, **111**, 6810.
9   T. R. Cook, Y.-R. Zheng and P. J. Stang, *Chem. Rev.*, 2013, **113**, 734, and references therein.
10 H.-B. Yang, K. Ghosh, Y. Zhao, B. H. Northrop, M. M. Lyndon, D. C. Muddiman, H. S. White and P. J. Stang, *J. Am. Chem. Soc.*, 2008, **130**, 839.
11 J.-K. Ou-Yang, L.-J. Chen, L. Xu, C.-H. Wang, H.-B. Yang, *Chin. Chem. Lett.*, 2013, **24**, 471.
12 L. G. Vaughan, *J. Am. Chem. Soc.*, 1970, **92**, 730.
13 H. Jude, H. Disteldorf, S. Fischer, T. Wedge, A. M. Hawkridge, A. M. Arif, M. F. Hawthorne, D. C. Muddiman and P. J. Stang, *J. Am. Chem. Soc.*, 2005, **127**, 12131.
14 G.-Z. Zhao, Q.-J. Li, L.-J. Chen, H. Tan, C.-H. Wang, D. A. Lehman, D. C. Muddiman and H.-B. Yang, *Organometallics*, 2011, **30**, 3637.
15 K. Ghosh, Y. Zhao, H.-B. Yang, B. H. Northrop, H. S. White and P. J. Stang, *J. Org. Chem.*, 2008, **73**, 8553.
16 G. R. Newkome, F. Moorefield, G. R. Baker, A. L. Johnson and R. K. Behera, *Angew. Chem. Int. Ed.*, 1991, **30**, 1176.
17 Q. Han, Q.-J. Li, J. He, B. Hu, H. Tan, Z. Abliz, C.-H. Wang, Y. Yu and H.-B. Yang, *J. Org. Chem.*, 2011, **76**, 9660.
18 Q.-J. Li, G.-Z. Zhao, L.-J. Chen, H. Tan, C.-H. Wang, D.-X. Wang, D. A. Lehman, D. C. Muddiman and H.-B. Yang, *Organometallics*, 2012, **31**, 7241.
19 G.-Z. Zhao, L.-J. Chen, C.-H. Wang, H.-B. Yang, K. Ghosh, Y.-R. Zheng, M. M. Lyndon, D. C. Muddiman and P. J. Stang, *Organometallics*, 2010, **29**, 6137.
20 N. Das, P. S. Mukherjee, A. M. Arif and P. J. Stang, *J. Am. Chem. Soc.*, 2003, **125**, 13950.
21 G.-Z. Zhao, Q.-J. Li, L.-J. Chen, H. Tan, C.-H. Wang, D.-X. Wang and H.-B. Yang, *Organometallics*, 2011, **30**, 5141.
22 C. J. Pedersen, *J. Am. Chem. Soc.*, 1967, **89**, 7017.
23 F. Huang, D. S. Nagvekar, C. Slebodnick and H. W. Gibson, *J. Am. Chem. Soc.*, 2005, **127**, 484.
24 K. Ghosh, J. Hu, H.-B. Yang, B. H. Northrop, H. S. White and P. J. Stang, *J. Org. Chem.*, 2009, **74**, 4828.
25 L.-J. Chen, Q.-J. Li, J. He, H. Tan, Z. Abliz and H.-B. Yang, *J. Org. Chem.*, 2012, **77**, 1148.
26 C.-C. You and F. Würthner, *J. Am. Chem. Soc.*, 2003, **125**, 9716.
27 N. Das, A. M. Arif and P. J. Stang, *Inorg. Chem.*, 2005, **44**, 5798.
28 M. Li, P. Cai, C. Duan, F. Lu, J. Xie and Q. Meng, *Inorg. Chem.*, 2004, **43**, 5174.
29 M. Wenzel, J. R. Hiscock and P. A. Gale, *Chem. Soc. Rev.*, 2012, **41**, 480.
30 L.-Y. Yao, L. Qin, T.-Z. Xie, Y.-Z. Li and S.-Y. Yu, *Inorg. Chem.*, 2011, **50**, 6055.
31 L.-Y. Yao, Z.-S. Yu, L. Qin, Y.-Z. Li, Y. Qin and S.-Y. Yu, *Dalton Trans.*, 2013, **42**, 3447.
32 O. Shoji, S. Okada, A. Satake and Y. Kobuke, *J. Am. Chem. Soc.*, 2005, **127**, 2201.
33 P. J. Stang, B. Olenyuk, J. Fan and A. M. Arif, *Organometallics*, 1996, **15**, 904.
34 V. Vajpayee, H. Kim, A. Mishra, P. S. Mukherjee, P. J. Stang, M. H. Lee, H. K. Kim and K.-W. Chi, *Dalton Trans.*, 2011, **40**, 3112.
35 S. Ghosh and P. S. Mukherjee, *Inorg. Chem.*, 2009, **48**, 2605.
36 A. K. Bar, R. Chakrabarty and P. S. Mukherjee, *Organometallics*, 2008, **27**, 3806.
37 S.-S. Sun, J. A. Anspach and A. J. Lees, *Inorg. Chem.*, 2002, **41**, 1862.
38 S.-S. Sun and A. J. Lees, *Inorg. Chem.*, 2001, **40**, 3154, and references therein.
39 S.-S. Sun, J. A. Anspach, A. J. Lees and P. Y. Zavalij, *Organometallics*, 2002, **21**, 685.
40 A. Mishra, S. Ravikumar, S. H. Hong, H. Kim, V. Vajpayee, H. Lee, B. Ahn, M. Wang, P. J. Stang and K.-W. Chi, *Organometallics*, 2011, **30**, 6343, and references therein.
41 K. Ghosh, J. Hu, H. S. White and P. J. Stang, *J. Am. Chem. Soc.*, 2009, **131**, 6695.
42 J. E. M. Lewis, A. B. S. Elliott, C. J. McAdam, K. C. Gordon and J. D. Crowley, *Chem. Sci.*, 2014, **5**, 1833.
43 Y.-R. Zheng, Z. Zhao, M. Wang, K. Ghosh, J. B. Pollock, T. R. Cook and P. J. Stang, *J. Am. Chem. Soc.*, 2010, **132**, 16873.
44 M. Wang, Y.-R. Zheng, T. R. Cook and P. J. Stang, *Inorg. Chem.*, 2011, **50**, 6107.
45 M. Wang, W.-J. Lan, Y.-R. Zheng, T. R. Cook, H. S. White and P. J. Stang, *J. Am. Chem. Soc.*, 2011, **133**, 10752.
46 J. S. Mugridge, D. Fiedler and K. N. Raymond, *J. Coord. Chem.*, 2010, **63**, 2779.

47 F. Jiang, J. Wang, J. Li, N. Wang, X. Bao, T. Wang, Y. Yang, Z. Lan and R. Yang, *Eur. J. Inorg. Chem.*, 2013, 375.

48 S.-S. Sun, J. A. Anspach, A. J. Lees, *Inorg. Chim. Acta*, 2003, **351**, 363.

5 49 S. Goeb, S. Bivaud, V. Croué, V. Vajpayee, M. Allain and M. Sallé, *Materials*, 2014, **7**, 611.

50 A. K. Bar, R. Chakrabarty, G. Mostafa and P. S. Mukherjee, *Angew. Chem. Int. Ed.*, 2008, **47**, 8455.

10 **The Brief Biographies of Authors**

Lin Xu

Lin Xu received his PhD degree in chemistry from the East China University of Science and Technology (ECUST, Shanghai) in 2012 under the supervision of Professor Xuhong Qian. 15 Subsequently, he joined the East China Normal University (ECNU, Shanghai) as an assistant professor and was promoted to associate professor in 2014. His research interests focus mainly on supramolecular self-assembly and fluorescence sensing.
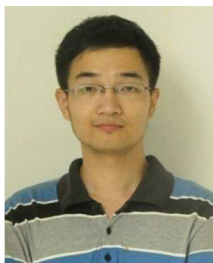
Yu-Xuan Wang

20 Yu-Xuan Wang received his BS degree in chemistry from Beijing Normal University in 2013. He is currently pursuing his MS degree in the laboratory of Prof. Hai-Bo Yang at ECNU. His current research interests are focused on the preparation of chiral metallacycles via coordination-driven self-assembly and their 25 applications in catalysis, sensing, etc.

30

Li-Jun Chen

35 Li-Jun Chen received her BS degree in chemistry from ECNU in 2010. Then she joined Prof. Hai-Bo Yang's group at ECNU to pursue her Ph.D. degree in chemistry. Her current research interests are focused on controllable self-assembly based on 40 organometallic metallacycles.

Hai-Bo Yang

Hai-Bo Yang obtained his Ph.D. degree at the Institute of Chemistry, Chinese Academy of Sciences (ICCAS) in Beijing in 2004. Then he joined Professor Peter J. Stang's group at 45 University of Utah as a Postdoctoral Fellow. Since the end of 2008, he has started his independent research as a PI at East China Normal University in Shanghai. Prof. Yang's research interests span the areas of organic, organometallic, and supramolecular chemistry.